Oxidopyridinium Cycloadditions Revisited: A Combined Computational and Experimental Study on the Reactivity of 1-(2-Pyrimidyl)-3-oxidopyridinium Betaine

Yoshihiko Yamamoto,* Yudai Shizume, Syunji Tazawa, and Takeshi Yasui

Department of Basic Medicinal Sciences, Graduate School of Pharmaceutical Sciences, Nagoya University, Chikusa, Nagoya 464-8601, Japan

*yamamoto-yoshi@ps.nagoya-u.ac.jp

Graphic Abstract

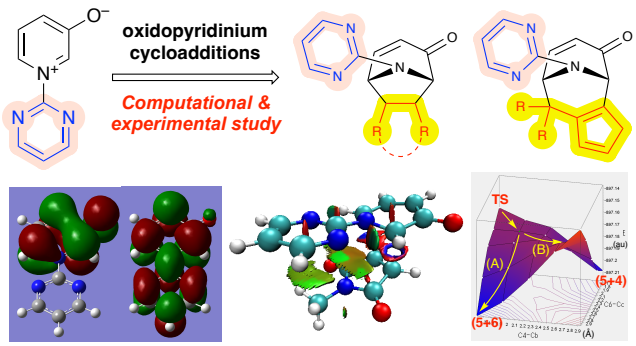

Abstract: To investigate the effect of *N*-substituents on their reactivity and selectivity of oxidopyridinium betaines, we performed density functional theory (DFT) calculations of model cycloadditions with *N*-methylmaleimide and acenaphthylene. The theoretically expected results were compared with the experimental results. Subsequently, we demonstrated that 1-(2-pyrimidyl)-3-oxidopyridinium can be used for (5+2) cycloadditions with various electron-deficient alkenes, dimethyl acetylenedicarboxylate, acenaphthylene, and styrene. In addition, a DFT analysis of the cycloaddition of 1-(2-pyrimidyl)-3-oxidopyridinium with 6,6-dimethylpentafulvene suggested the possibility of a pathway bifurcations involving a (5+4)/(5+6) ambimodal transition states, although only (5+6) cycloadducts were experimentally observed. A related (5+4) cycloaddition was observed in the reaction of 1-(2-pyrimidyl)-3-oxidopyridinium with 2,3-dimethylbut-1,3-diene.

Key words: Cycloaddition; DFT calculation; Oxidopyridinium; Azabicyclic compound

Introduction

Since the pioneering studies by the Katritzky group,[1] the (5+2) cycloaddition of oxidopyridinium betaines with dipolarophiles has been extensively investigated because it provides straightforward access to the tropane framework, which is found in cocaine and related bioactive compounds (Figure 1a).[2,3] In addition, oxidopyridinium (5+2) cycloadditions have been utilized for the synthesis of natural product-like tropane scaffolds,[4] as well as complex natural products.[5]

Katritzky and Takeuchi reported that 1-methyl-3-oxidopyridinium reacted with electron-deficient alkenes, such as methyl acrylate and *N*-phenylmaleimide, at elevated temperatures to afford the corresponding (5+2) cycloadducts (Figure 1b).[6] Although the reaction with methyl acrylate resulted in the formation of a mixture of *exo*- and *endo*-adducts, the reaction with *N*-phenylmaleimide selectively produced an *exo*-adduct. Later, Katritzky *et al.* found that oxidopyridinium betaines bearing 5-nitro-2-pyridyl and 4,5-dimethyl-2-pyrimidyl groups on the nitrogen atom exhibited different reactivities with the *N*-methyl derivative;[7] in addition to electron-deficient alkenes, styrene reacted with

these 1-azinyl-3-oxidopyridiniums at 90 °C to selectively produce the corresponding *endo*-adducts. Moreover, 1-azinyl-3-oxidopyridiniums participated in the (5+4) cycloaddition with 1,3-butadienes, and the (5+6) cycloaddition took place with pentafulvenes even at 20 °C.[6] Accordingly, the product selectivity varied depending on the combination of oxidopyridinium betaines with dipolarophiles as well as reaction conditions; thus, the direct comparison of the reactivities of oxidopyridinium betaines is difficult.

To gain insight into the effect of *N*-substituents, we performed a combined computational and experimental study on the cycloaddition of oxidopyridinium betaines. We investigated the reactivities of betaines bearing methyl, 2-pyrimidyl, and 5-nitro-2-pyridyl groups on the nitrogen atom using density functional theory (DFT) calculations, and the obtained results were compared with those of the experimental study to identify an optimal *N*-substituent. Furthermore, the reactions of the optimal oxidopyridinium with various dipolarophiles were investigated both computationally and experimentally to expand the scope. The present study demonstrates that 1-(2-pyrimidyl)-3-oxidopyridinium participates in (5+2) cycloadditions with electron-deficient alkenes and

arylalkenes as well as other types of cycloadditions.

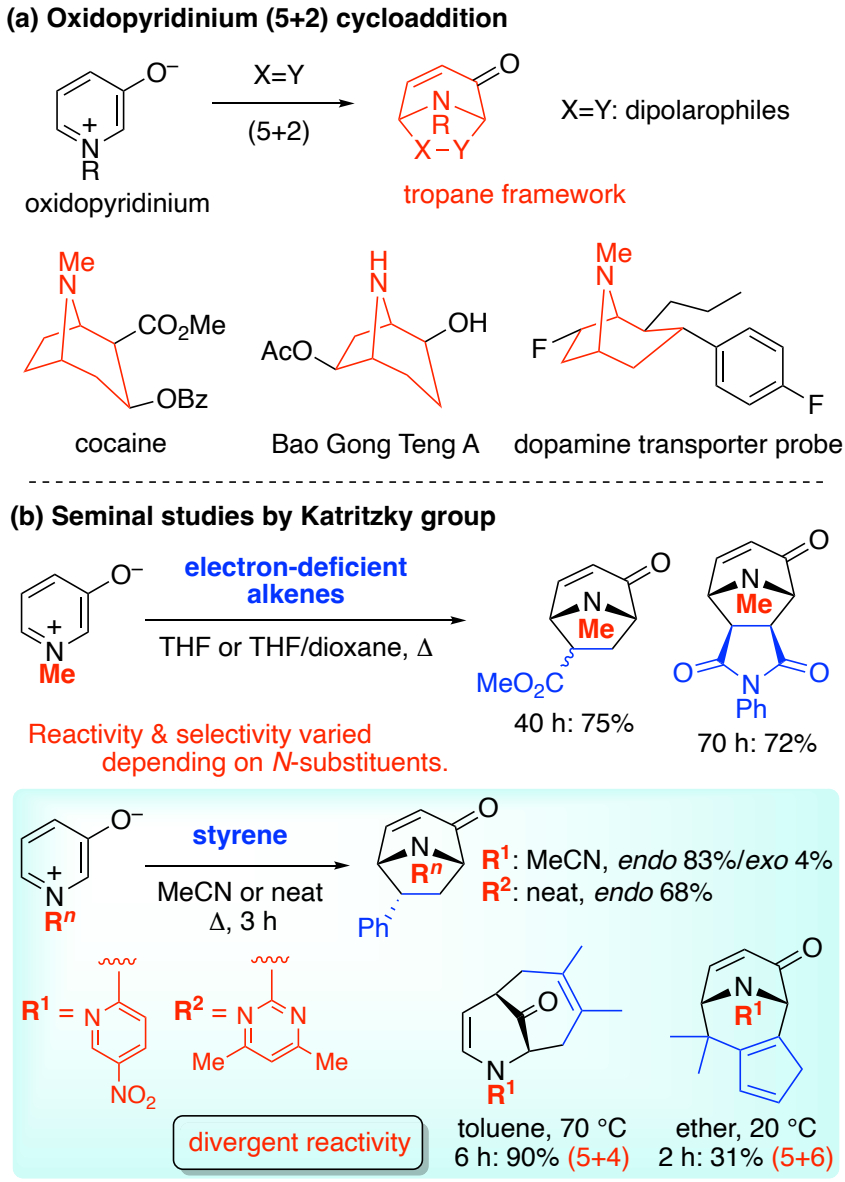

Figure 1. (a) Oxidopyridinium (5+2) cycloaddition and related tropanes and (b) Katritzky's pioneering studies.

Results and Discussion

Initial computational analysis of oxidopyridinium betaines. Initially, we analyzed the oxidopyridinium betaines **1a**–**c** bearing *N*-methyl and *N*-azinyl groups by performing DFT calculations at the SMD (toluene) ωB97X-D/6-31G(d) level of theory. We investigated 1-(2-pyrimidyl)-3-oxidopyridinium (**1b**) as a model betaine instead of the 4,6-dimethylpyrimidyl-substituted analog used by the Katritzky group to eliminate the steric influence of the methyl groups on the pyrimidyl moiety.[7] The cycloaddition of **1b** with pentafulvenes was reported by Radhakrishnan and coworkers.[8] The oxidopyridinium moieties of **1a**–**c** have similar structural parameters, as shown in Figure 2a. Although **1b** has a planar geometry, the oxidopyridinium moiety and *N*-pyridine ring are not on the same plane in **1c**, because of the steric repulsion of the *ortho* C–H bonds. Accordingly, two stable conformers exist for **1c**; conformer **1c**-rot is slightly less stable than the major conformer (**1c**). Figure 2b shows orbital interaction diagrams for the reactions of oxidopyridinium betaines **1a** and **1b** with *N*-methylmaleimide (**2a**) and acenaphthylene (**2b**). The energy levels of the highest occupied molecular orbitals (HOMOs) of **1a** and **1b** are very similar (–6.98 and –6.95 eV, respectively), while the

lowest unoccupied molecular orbital (LUMO) of **1b** (–0.28 eV) is located significantly lower than that of **1a** (+0.72 eV). The low LUMO level of **1b** is ascribed to the conjugation of the *N*-pyrimidyl group, since the LUMO spreads over the pyrimidine π-orbitals. This contrasts with the HOMO of **1b**, which is confined to the pyridine π-orbitals. As a result, the HOMO (acenaphthylene)–LUMO (betaine) energy gap decreases from 8.62 eV with **1a** to 7.62 eV with **1b**. The LUMO level is further lowered to –1.26 eV for **1c**, and thus, the reaction with acenaphthylene should be more efficient for **1c** than for **1b**. However, the HOMO level of **1c** is also lowered (–7.22 eV), decreasing its reactivity toward electron-deficient alkenes, such as *N*-methylmaleimide.

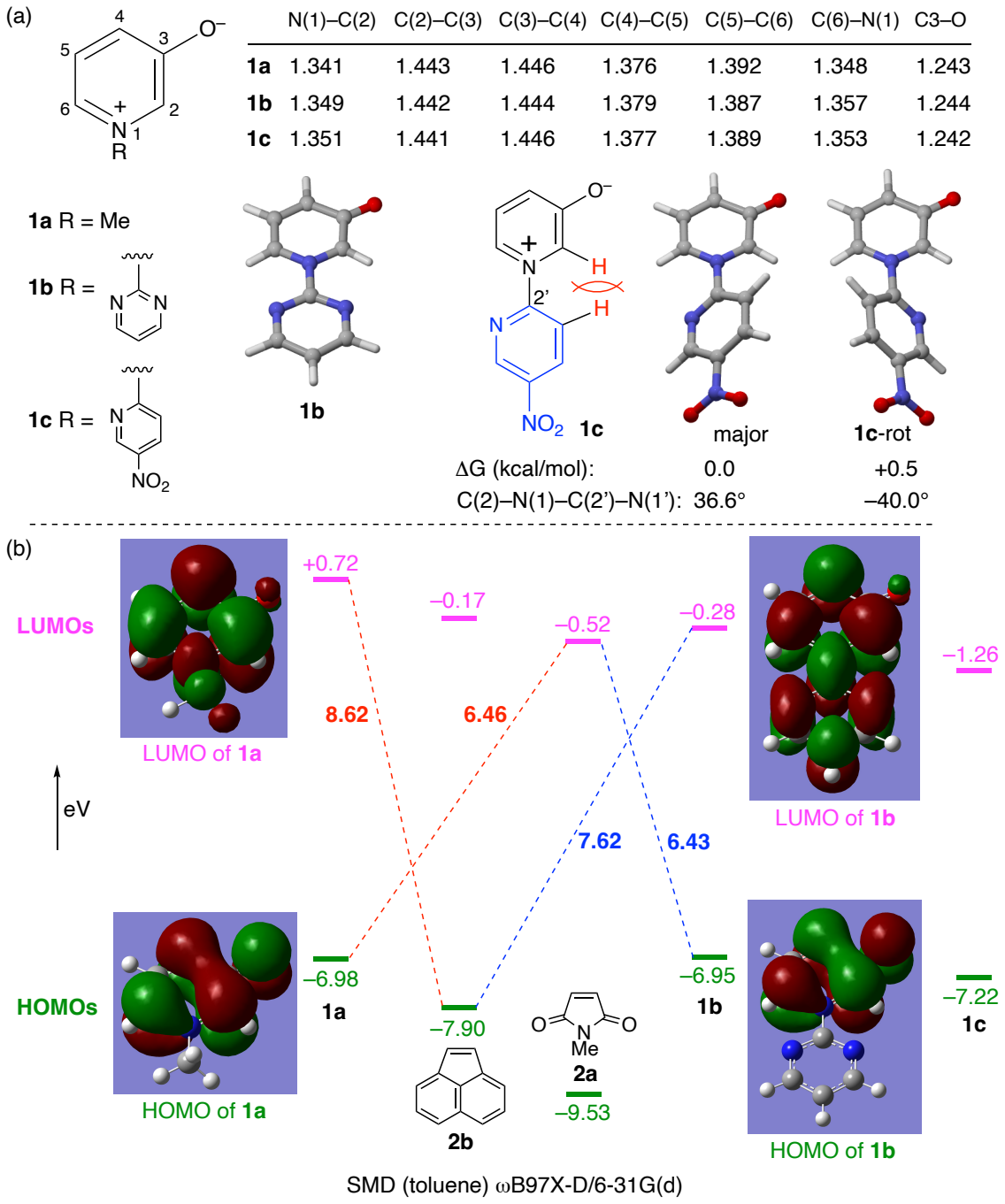

Figure 2. (a) Structural parameters of betaines **1a**–**c** and (b) orbital interaction diagram for the cycloadditions of **1a** and **1b** with *N*-methylmaleimide (**2a**) and acenaphthylene (**2b**).

To investigate the effect of *N*-substituents on their reactivity and selectivity of oxidopyridinium betaines, we performed DFT calculations of model cycloadditions with *N*-methylmaleimide (**2a**) and acenaphthylene (**2b**) at the SMD (toluene) M06-2x/6-311+G(2df,2p)//SMD (toluene) ωB97X-D/6-31G(d) level of theory.[9] Figure 3a shows the energy profile of the reaction of 1-methyl-3-oxidopyridinium (**1a**) with *N*-methylmaleimide (**2a**) as an electron-deficient dipolarophile. The (5+2) cycloaddition proceeds via asynchronous concerted transition states (TSs), in which the C(2)–C(a) distance is shorter than the C(6)–C(b) distance and the activation barriers are approximately 25 kcal/mol. The activation barriers are lower for *exo*-TS (**TS*exo*-Ia**) than for *endo*-TS (**TS*endo*-Ia**) by 1.5 kcal/mol, suggesting the formation of *exo*-**3aa** should be kinetically favored. The formations of cycloadducts *exo*-**3aa** and *endo*-**3aa** are exergonic by 5.1 and 3.6 kcal/mol, respectively; thus, the former is thermodynamically favored. Then, the reactions of 1-azinyl-3-oxidopyridiniums with **2a** were analyzed, and the obtained reaction parameters were compared with those of the above reaction (Table 1). The activation barriers decrease by ca. 3 kcal/mol when **1a** is replaced by **1b** (entries 1

and 2). More importantly, the reaction of **1b** is thermodynamically much more favored than that of **1a**, as shown by the higher exergonicity of the former. However, the difference in the activation barriers for the *exo*- and *endo*-TSs is smaller for the reaction of **1b** ($\Delta\Delta G^{\ddagger}$ = 0.5 kcal/mol) than for that of **1a** ($\Delta\Delta G^{\ddagger}$ = 1.5 kcal/mol), implying that the reaction of **1b** is less stereoselective. Similar reaction parameters were obtained when **1c** was used as the betaine (entry 3).

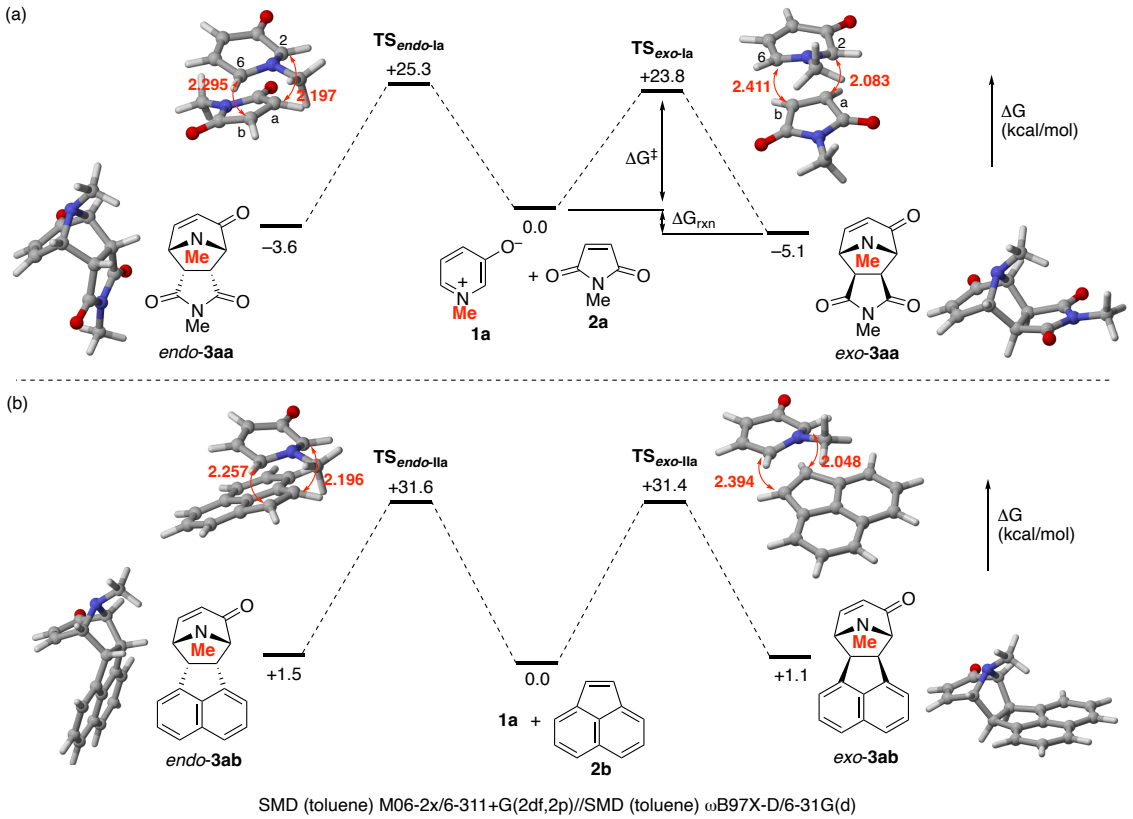

Figure 3. Energy profile for the (5+2) cycloaddition of oxidopyridinium betaine **1a** with

relative Gibbs energies (298 K, 1 atm) and interatomic distances (Å): (a) reaction with *N*-methylmaleimide (**2a**) and (b) reaction with acenaphthylene (**2b**).

Table 1. Reaction parameters (kcal/mol) for the reactions of oxidopyridinium betaines **1a**–**c** with *N*-methylmaleimide (**2a**) and acenaphthylene (**2b**).

entry	betaine	alkene	*exo*/$\Delta G^{\ddagger}$, ΔG_{rxn}	*endo*/$\Delta G^{\ddagger}$, ΔG_{rxn}
1	**1a**	**2a**	+23.8, –5.1	+25.3, –3.6
2	**1b**	**2a**	+21.1, –20.0	+21.6, –15.4
3	**1c**	**2a**	+20.4, –20.2	+21.1, –18.2
4	**1a**	**2b**	+31.4, +1.1	+31.6, +1.5
5	**1b**	**2b**	+25.6, –13.7	+27.0, –12.5
6	**1c**	**2b**	+23.7, –17.1	+25.7, –15.3

To gain insight into the TS structures, distortion/interaction analysis was applied to the cycloadditions of **1a** and **1b** with imide **2a** (Figure 4a).[10] The distortion energies of the betaine fragments (blue) are higher than those of the imide fragments (green) in all

TSs. The total distortion energies are higher for *endo*-TSs than for *exo*-TSs. **TS*exo*-Ib** and **TS*endo*-Ib** are earlier TSs than **TS*exo*-Ia** and **TS*endo*-Ia**, respectively, as evidenced by longer incipient bond distances of **TS*exo*-Ib** and **TS*endo*-Ib**. In line with this analysis, the distortion energies are significantly lower in **TS*exo*-Ib** and **TS*endo*-Ib** than in **TS*exo*-Ia** and **TS*endo*-Ia**. Furthermore, non-covalent interaction (NCI) analysis was performed for these TSs (Figure 4b).[11] In **TS*exo*-Ia**, a green area showing van der Waals interactions was observed between the *N*-methyl group of **1a** and the OC–N–CO moiety of **2a**. Similar attractive interactions were observed betweeen the *N*-pyrimidyl substituent of **1b** and **2a** in **TS*exo*-Ib**. Moreover, **TS*exo*-Ib** showed additional attractive interactions between the pyrimidyl ring and the *N*-methyl substituent of **2a**. Therefore, these attractive interactions contribute to lowering the activation barrier for **TS*exo*-Ib.** The similar van der Waals interactions between the enone moiety of **1a** or **1b** and the OC–N–CO moiety of **2a** are also observed. The *exo*/*endo* selectivity varies depending on the balance between these attractive interactions and other repulsive ones (vide infra).

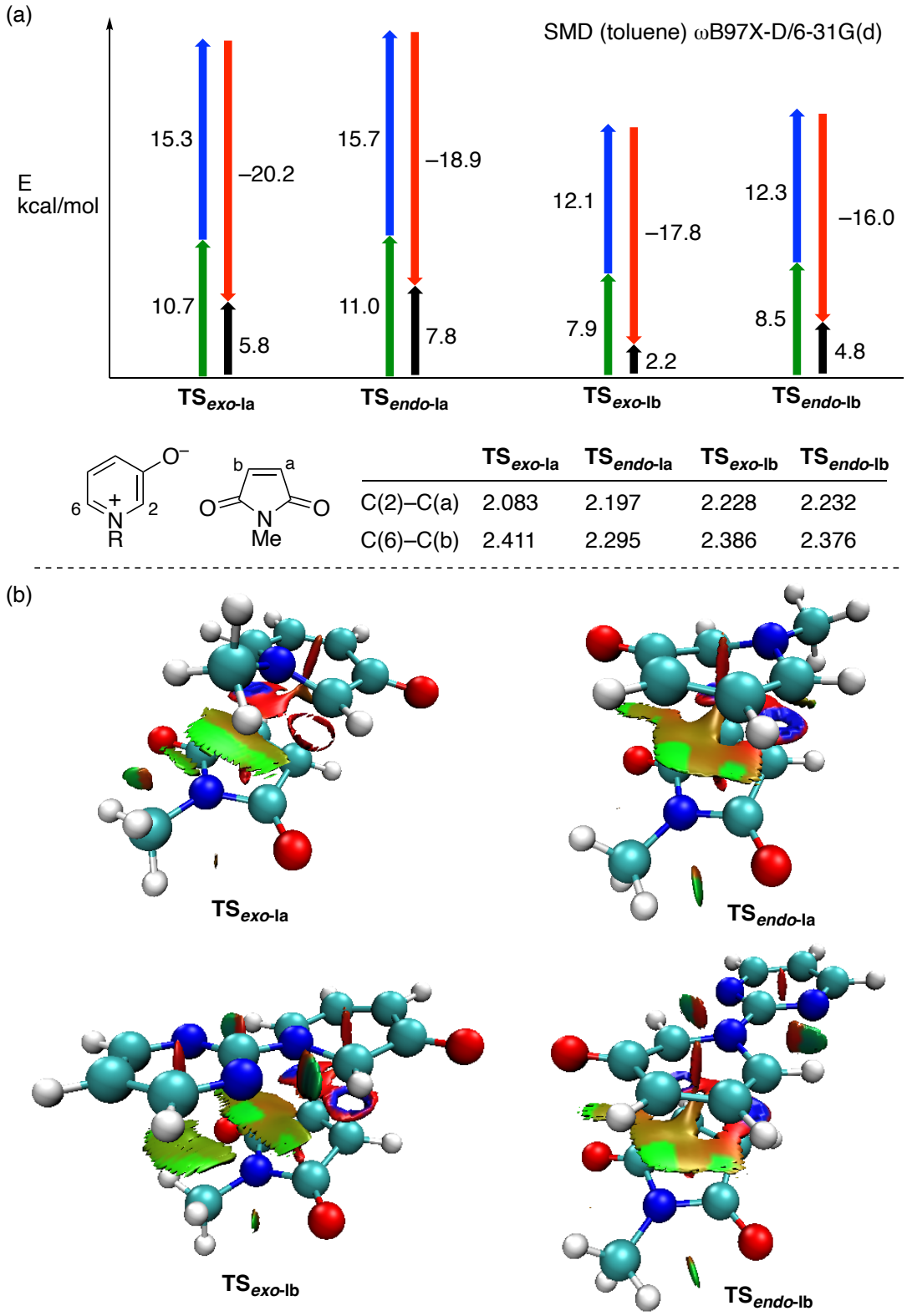

	$TS_{exo\text{-}Ia}$	$TS_{endo\text{-}Ia}$	$TS_{exo\text{-}Ib}$	$TS_{endo\text{-}Ib}$
C(2)–C(a)	2.083	2.197	2.228	2.232
C(6)–C(b)	2.411	2.295	2.386	2.376

Figure 4. (a) Distortion/interaction analysis for cycloadditions of betaines **1a** and **1b** with

maleimide **2a** (blue: distortion energy of betaine, green: distortion energy of imide, red: interaction energy, and black: activation energy), and (b) noncovalent interactions in **TS*exo*-Ia**, **TS*endo*-Ia**, **TS*exo*-Ib**, and **TS*endo*-Ib**.

DFT calculations suggest that the reaction of **1a** with a conjugated alkene, acenaphthylene (**2b**), is infeasible because the activation barriers are too high to overcome (ca. 31 kcal/mol) and the formations of cycloadducts are slightly endergonic (Figure 3b). Nevertheless, the activation barriers significantly decrease from ca. 31 kcal/mol to 25.6–27.0 kcal/mol when **1a** is replaced by **1b** (Table 1, entries 4 and 5). Moreover, the formations of the corresponding cycloadducts become exergonic. Therefore, the cycloaddition of **1b** with **2b** is expected to proceed at elevated temperatures. The activation barriers are further reduced in the cycloaddition of **1c** with **2b** (entry 6).

Experimental assessment of the reactivities of oxidopyridinium betaines toward representative dipolarophiles. The (5+2) cycloaddition of oxidopyridinium betaines was experimentally investigated using maleimide **2a** as an electron-deficient

dipolarophile. Commercially available pyridine-3-ol was treated with iodomethane (3 equiv) in dry acetone at 50 °C for 3 h, and evaporation of the solvent afforded crude pyridinium salt **1a**-H (Scheme 1a). Because **1a**-H is highly hygroscopic, the crude salt was directly used for the subsequent reaction. In the presence of **2a** (1 equiv), crude **1a**-H was treated with triethylamine (2 equiv) in dry toluene at 110 °C overnight (16 h), affording the desired cycloadduct *exo*-**3aa** in 77% yield. The high *exo*-selectivity is in good accordance with that previously reported by the Katritzky group.[6] In contrast, no reaction occurred when the reaction of **1a**-H with acenaphthylene (**2b**) was conducted in a similar manner.

The reactivity of *N*-(2-pyrymidyl)-substituted betaine **1b** was investigated using pyridinium salt **1b**-H as the precursor, which was prepared through the reaction of pyridine-3-ol with 2-chloropyrimidine in chlorobenzene at 120 °C for 5 h.[12] In the presence of **2a** (1 equiv), **1b**-H (0.3 mmol) was treated with triethylamine (2 equiv) in toluene at 110 °C for 16 h, affording *exo*- and *endo*-**3ba** with the *exo*/*endo* ratio of 6:1 (Scheme 1b). After purification by silica-gel column chromatography, *exo*-**3ba** was obtained in 77% yield (*exo*/*endo* >10:1). The same reaction was performed on a 1 mmol

scale to afford *exo*-**3ba** in 70% yield after recrystallization. The higher reactivity of **1b** than **1a** toward conjugated alkene **2b** was demonstrated by the formation of *exo*-**3bb**, albeit in a low yield (ca. 10%) under similar conditions. Moreover, the reaction of **1b**-H with **2b** was conducted at a higher temperature (130 °C) in xylene, affording **3bb** in 34% yield with an *exo*/*endo* ratio of 3.1:1. The yield of **3bb** further improved to 67% when the loading of **2b** was increased to three equivalents.

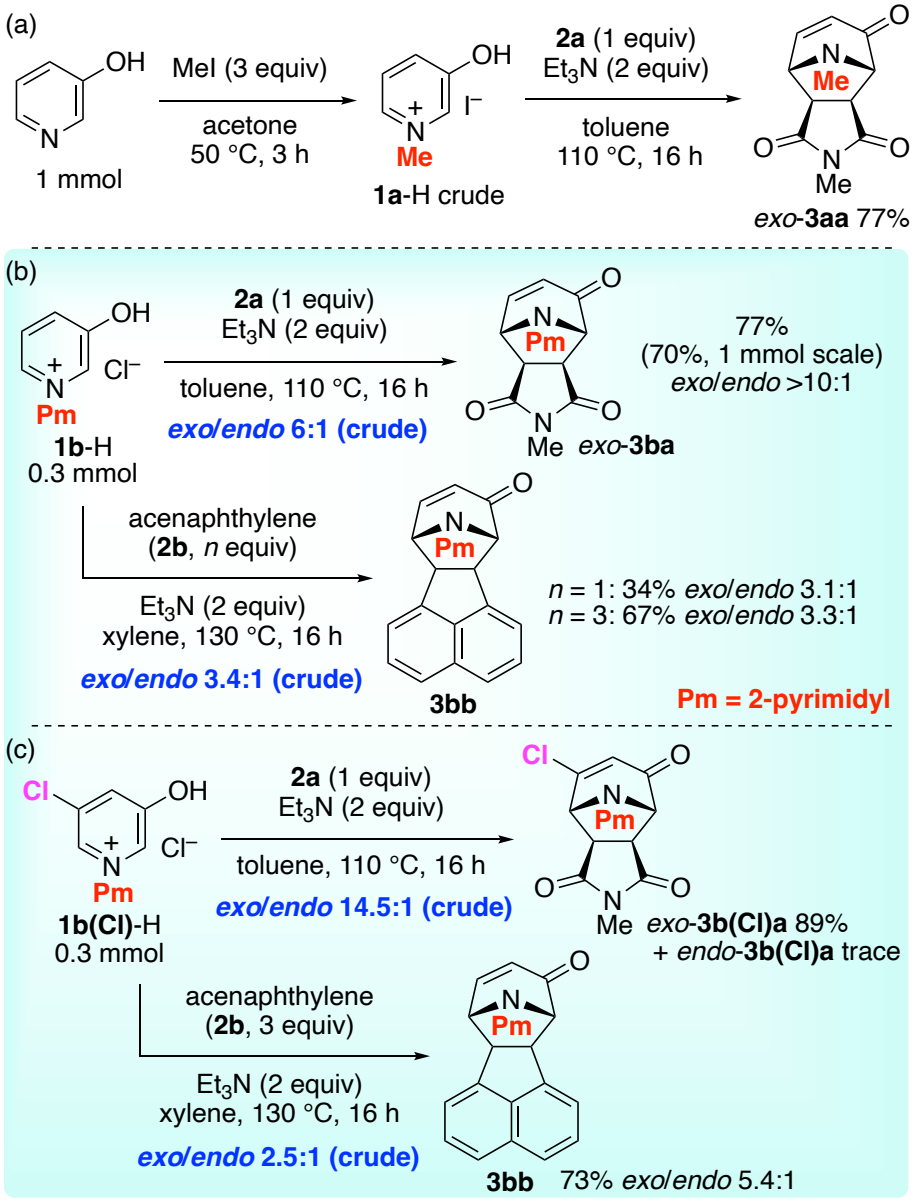

Scheme 1. (a) Reaction of **1a**-H with *N*-methylmaleimide (**2a**), (b) reaction of **1b**-H with **2a** and acenaphthylene (**2b**), and (c) reaction of **1b(Cl)**-H with **2a** and **2b**.

Although the experimental stereoselectivity (crude *exo*/*endo* = 6:1) observed in the reaction of **1b**-H with **2a** was higher than that predicted by the above DFT analysis (*exo*/*endo* = 2.3:1, Table 1), calculations at a higher theory level [M06-2X(D3)/6-

311+G(2df,2p)//ωB97X-D/6-31+G(d,p)] successfully reproduced the experimental *exo*/*endo* ratio (6.1:1, Figure S1a in the Supporting Information). The M06-2X/6-311+G(2df,2p)//ωB97X-D/6-31G(d) method predicted the lower *exo*/*endo* ratio, probably because the electrostatic repulsion between the enone carbonyl moiety of the betaine and one of the imide carbonyls is underestimated; the C(3)–C(c) and C(5)–C(d) distances in **TS*endo*-Ib** elongated at the higher theory level [M06-2X(D3)/6-311+G(2df,2p)//ωB97X-D/6-31+G(d,p)] (Figure S1c). In contrast, the experimental stereoselectivity (crude *exo*/*endo* = 3.4:1) observed in the reaction of **1b**-H with **2b** was lower than that predicted by the DFT analysis (*exo*/*endo* = 10.6:1, Table 1), and calculations at the higher theory level also failed to reproduce the experimental *exo*/*endo* ratio (Figure S1b). Therefore, the theoretical prediction of the stereoselectivity in the reaction of **1b** with **2b** needs further improvements.

In line with the above considerations, the reaction of **1b(Cl)**-H with imide **2a** afforded *exo*/*endo*-**3b(Cl)a** in a much higher *exo*/*endo* ratio of 14.5:1 (Scheme 1c). The DFT calculations predicted the $\Delta\Delta G^{\ddagger}$ value of 2.2 kcal/mol, in favor of the *exo*-TS (Figure S2a in the Supporting Information), which is much higher than the $\Delta\Delta G^{\ddagger}$ value predicted

for the reaction of **1b**-H with **2a** (0.6 kcal/mol). The improved stereoselectivity is ascribed to the additional electrostatic repulsion between the chlorine substituent and imide carbonyl group as demonstrated by the incresed C(5)–C(d) distance in **TS*endo*-1b(Cl)** (Figure S1c). In contrast, the reaction of **1b(Cl)**-H with acenaphthylene (**2b**) afforded an *exo*/*endo* ratio of 2.5:1, which is slightly lower than that observed in the reaction of **1b**-H with **2b**. The calculated $\Delta\Delta G^{\ddagger}$ value (0.9 kcal/mol) is lower than that predicted for the reaction of **1b** with **2b** (1.4 kcal/mol) as shown in Figure S2b.

Subsequently, the reaction of 1-(5-nitro-2-pyridyl)-analog **1c** was investigated using precursor **1c**-H, which was prepared according to a previous report (3-hydroxypyridine, 2-chloro-5-nitropyridine, THF reflux).[12] Because the reported method required a long reaction time (113 h), the reaction of pyridine-3-ol with 2-chloro-5-nitropyridine was conducted at a higher temperature (120 °C) in chlorobenzene. However, the desired pyridinium salt was not obtained because of the N–to–O migration of the 5-nitro-2-pyridyl group. This suggests that **1c**-H is unstable at high temperatures. The reaction of **1c**-H with **2a** was performed in a manner similar to that described above. Although the reaction efficiently proceeded, the expected product **3ca** was obtained with

a lower stereoselectivity of *exo*/*endo* 2.0:1 (Scheme S1a in the Supporting Information). Moreover, chromatographic purification was difficult because **3ca** is sparingly soluble in common organic solvents; *exo*- and *endo*-**3ca** were obtained as an inseparable mixture in a moderate yield (ca. 40%). Katritzky *et al.* reported that the betaine **1c**, which was derived from its dimer, reacted with maleic anhydride in 1,2-dichloroethane (DCE) under reflux to exclusively afford the corresponding *endo*-cycloadduct in 92% yield (Scheme S1b). Thus, the reaction of the dimer of **1c** with imide **2a** was conducted in toluene at 110 °C for 16 h (Scheme S1c). The ^{1}H NMR analysis of the crude product showed that *exo*/*endo*-**3c** was produced in 67% yield with the *exo*/*endo* ratio of 5.2:1. Therefore, the *exo*/*endo*-selectivity in the reaction of **1c** significantly varies, depending on the reaction partner used as well as reaction conditions. Although a higher reactivity of betaine **1c** than **1b** toward conjugated alkene **2b** was theoretically expected, the corresponding cycloadduct was hardly detected in the crude reaction mixture when the reaction of **1c**-H with **2b** was conducted in the presence of triethylamine (2 equiv) in toluene at 110 °C for 16 h. This unexpected result can be ascribed to the thermal instability of **1c** at elevated temperatures. The decomposition of **1c** is probably much faster than the cycloaddition of

1c with **2b**.

Scope of dipolarophiles in the (5+2) cycloaddition of 1-(2-pyrimidyl)-3-oxidopyridinium. Accordingly, **1b** is superior to **1c** in terms of thermal stability and stereoselectivity. Therefore, the reaction of **1b** with other dipolarophiles was further investigated using **1b**-H as the betaine precursor. In the presence of dimethyl maleate (**2c**, 2 equiv), **1b**-H was treated with triethylamine (2 equiv) in toluene at 110 °C to produce a complex product mixture (Scheme 2a). Chromatographic purification afforded *exo*-**3bc** in 25% yield along with an inseparable mixture of *endo*-**3bc** and two diastereomers derived from dimethyl fumarate. This result shows that triethylamine promotes the *Z–E* isomerization of maleate to produce fumarate (inset scheme).

To avoid *Z–E* isomerization, base-free conditions were examined. Katritzky *et al.* prepared dimers of 1-azinyl-3-oxidopyridinium betaines[12] and used them as sources of betaines.[7] According to their report, **1b**-H was treated with triethylamine (1.2 equiv) in 1,2-dichloroethane (DCE) at room temperature for 0.5 h, and the crude dimer was obtained after removal of the hydrochloride salt of triethylamine by filtration and

subsequent extraction with H_2O (Scheme 2b). A comparison of the ^1H NMR data of the crude dimer with that of the Katritzky's 1-(4,6-dimethyl-2-pyrimidyl-3-oxopyridinium betaine dimer suggests that *exo*-**4a** was formed almost exclusively along with trace amounts of *exo*-**4b**. This result is in good agreement with the results of DFT analysis of the dimerization of **1b** (Figure 5). The formation of *exo*-**4a** proceeds via **TS*exo*-IIIa** with the second lowest activation barrier of +19.0 kcal/mol, which can be overcome at room temperature. Although the activation barrier is the lowest, the formation of *endo*-**4a** is unfavorable because of its endergonicity. Therefore, *exo*-**4a** is thermodynamically favored. Although *exo*-**4b** is slightly more stable than *exo*-**4a**, the activation barrier of **TS*exo*-IIIb** is 2.7 kcal/mol higher than that of **TS*exo*-IIIa**. These theoretical results are in good accordance with Katritzky's observation that the major isomer corresponding to *exo*-**4a** underwent isomerization to the other isomer corresponding to *exo*-**4b** in $CDCl_3$.[12] The activation barrier of retro-dimerization of *exo*-**4a** is estimated as +26.3 kcal/mol, indicating that betaine **1b** can be generated from *exo*-**4a** at an elevated temperature. In striking contrast, the dimerization of betaine **1a** was theoretically predicted to be infeasible because of its high activation barriers (> +30 kcal/mol) and significant

endergonicity (> +20 kcal/mol), as shown in Figure S3 (Supporting Information).

In the presence of **2c** (2 equiv), crude *exo*-**4a** was heated in toluene at 110 °C for 16 h to afford *exo*-**3bc** in 41% yield (36% in two steps), and the formation of cycloadducts derived from fumarate was efficiently suppressed (Scheme 2b). Furthermore, a one-pot telescoping procedure was examined; **1b**-H was treated with triethylamine (1.2 equiv) in dry toluene at room temperature for 0.5 h, and subsequently, crude *exo*-**4a** was directly subjected to cycloaddition with maleate **2c** (2 equiv) at 110 °C for 16 h. Consequently, *exo*-**3bc** was obtained in an improved yield (40%), although the total amounts of *trans*-diastereomers increased. The direct reaction of **1b**-H with dimethyl acetylenedicarboxylate (DMAD, **2d**) in the presence of triethylamine afforded a complex reaction mixture. Therefore, this telescoping procedure was applied to the reaction with **2d** to afford **3bd** in 72% yield (Scheme 2c).

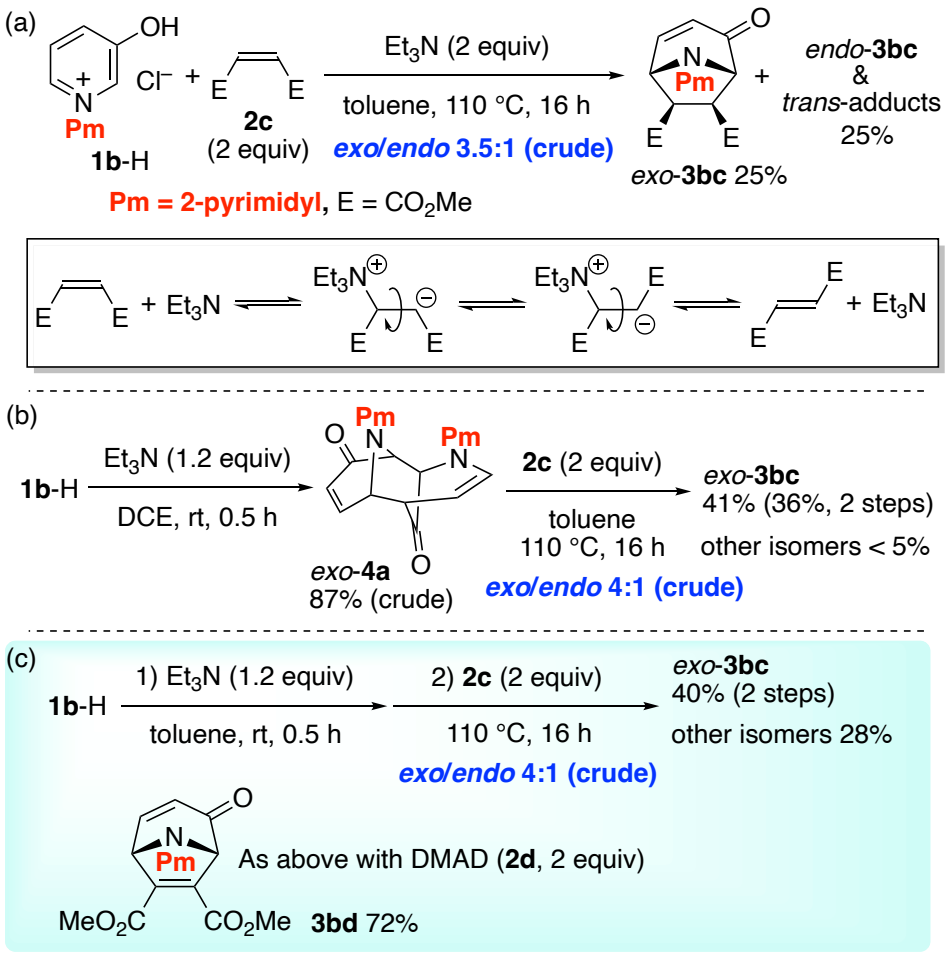

Scheme 2. (a) Reaction of betaine **1b**-H with dimethyl maleate (**2c**), (b) generation of betaine dimer *exo*-**4a** and its reaction with **2c**, and (c) one-pot reaction of **1b**-H with **2c** and DMAD (**2d**) via *exo*-**4a**.

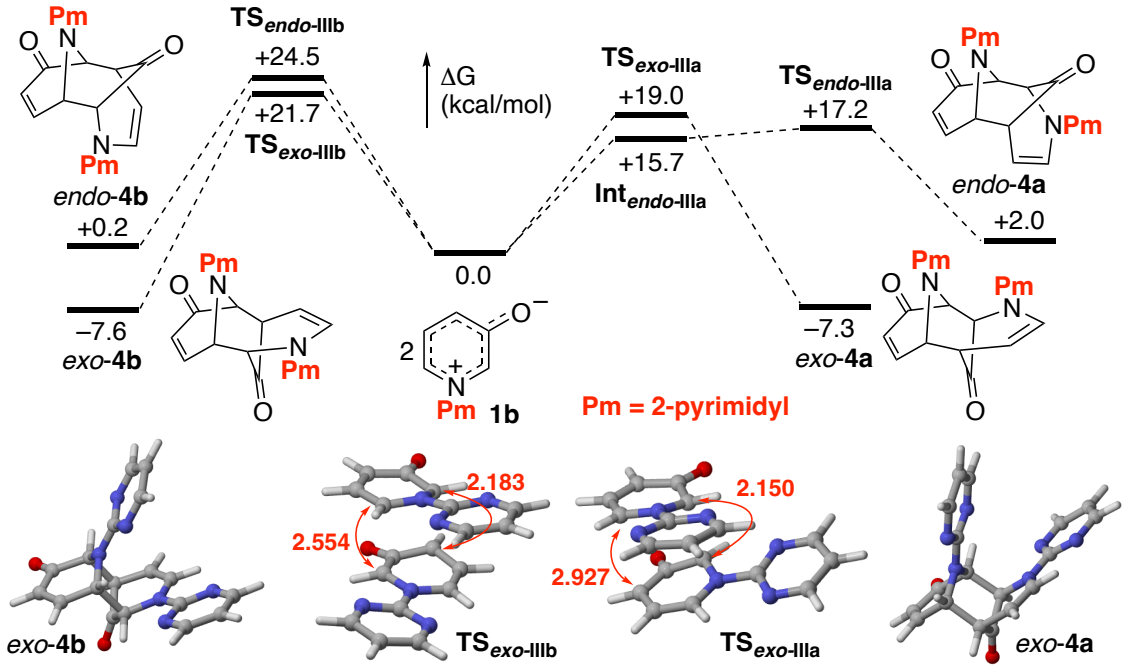

Figure 5. Energy profiles for the dimerization of betaine **1b** with relative Gibbs energies (298 K, 1 atm).

In their pioneering study, Katritzky *et al.* revealed that the dimer of betaine **1c** reacted with acrylonitrile, methyl vinyl ketone, and methyl acrylate to afford the corresponding *exo*/*endo*-cycloadducts with various stereoselectivities when electron-deficient alkenes were used as solvents (Scheme 3a).[7] However, phenyl vinyl sulfone has not been used as a dipolarophile for the cycloaddition of 1-azinyl-3-oxidopyridinium betaines, although its reactions with 1-alkyl-3-oxidopyridinium betaines gave the

corresponding products in good yields and selectivity.[13] In the presence of triethylamine (2 equiv), betaine precursor **1b**-H and vinyl sulfone **2e** (1 equiv) were heated in toluene at 110 °C for 16 h to afford a mixture of three cycloadduct isomers in a ratio of *exo*-**3be**:*endo*-**3be**:*exo*-**5be** ≥ 20:1:1 (Scheme 3b). Separation by silica gel chromatography afforded pure *exo*-**3be** in 76% yield. This result was nicely corroborated by DFT calculations, as shown in Figure 6. The formation of *exo*-**3be** is both kinetically and thermodynamically most favored among the four possible isomers. The theoretically predicted kinetic ratio of *exo*-**3be**:*endo*-**3be**:*exo*-**5be** = 68:3:1 is in good agreement with the experimentally observed ratio.

The reaction of betaine **1b** with methyl acrylate was also analyzed using DFT calculations, and the results are outlined in Figure S4 (Supporting Information). In this case, the activation barriers increase in the following order: **TS*exo*-sIIa** > **TS*endo*-sIIa** > **TS*endo*-sIIb** > **TS*exo*-sIIb**. The kinetic product ratio was calculated to be *exo*-**s2a**:*endo*-**s2a**:*endo*-**s2b**:*exo*-**s2b** = 84.6:13.1:1.8:0.5. Therefore, it was predicted that the reaction of **1b** with methyl acrylate would afford *exo*-**s2a** and *endo*-**s2a** in an 86.7:13.3 ratio. Therefore, these theoretical investigations demonstrate the excellent efficiency and

selectivity of phenyl vinyl sulfone (**2e**) as a dipolarophile for oxidopyridinium [5+2] cycloaddition.

As described in the introduction, Katritzky *et al.* reported high *endo*-selectivity for the cycloaddition of 1-azinyl-3-oxidopyridinium betaines with styrene (Figure 1b). Our DFT analysis of the reaction involving betaine **1b** and styrene led to similar results, indicating that the corresponding product *endo*-**3bf** is exclusively produced (Figure S5 in the Supporting Information). This *endo*-selectivity was also experimentally confirmed, as shown in Scheme 3c, although the observed stereoselectivity (*endo*:*exo* = 6:1) was significantly lower than that theoretically expected (*endo*:*exo* = 41:1). NCI analysis of **TS*endo*-sIIIa** and **TS*endo*-IIIb** showed that van der Waals interactions between the enone moiety of **1b** and arylalkenes are similar (Figure S6 in the Supporting Information). In **TS*exo*-sIIIa**, the pyrimidine ring slightly tilts to mitigate steric repulsions with the phenyl ring. As a consequence, van der Waals interactions between the pyrimidine ring of **1b** and arylalkenes is obviously much less extensive in **TS*exo*-sIIIa** than in **TS*exo*-IIIb**. Therefore, the *endo*-mode approach is favored for the reaction of **1b** with styrene, while acenaphthylene prefers the *exo*-mode approach.

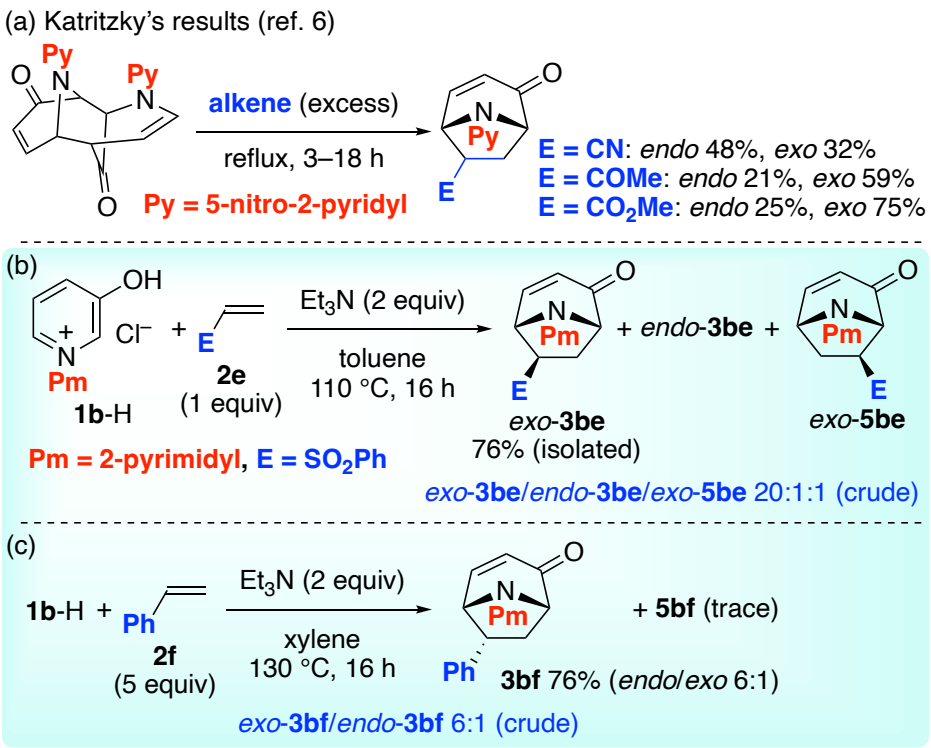

Scheme 3. (a) Katritzky's pioneering studies, (b) reaction of **1b**-H with phenyl vinyl sulfone (**2e**), and (c) reaction of **1b**-H with styrene (**2f**).

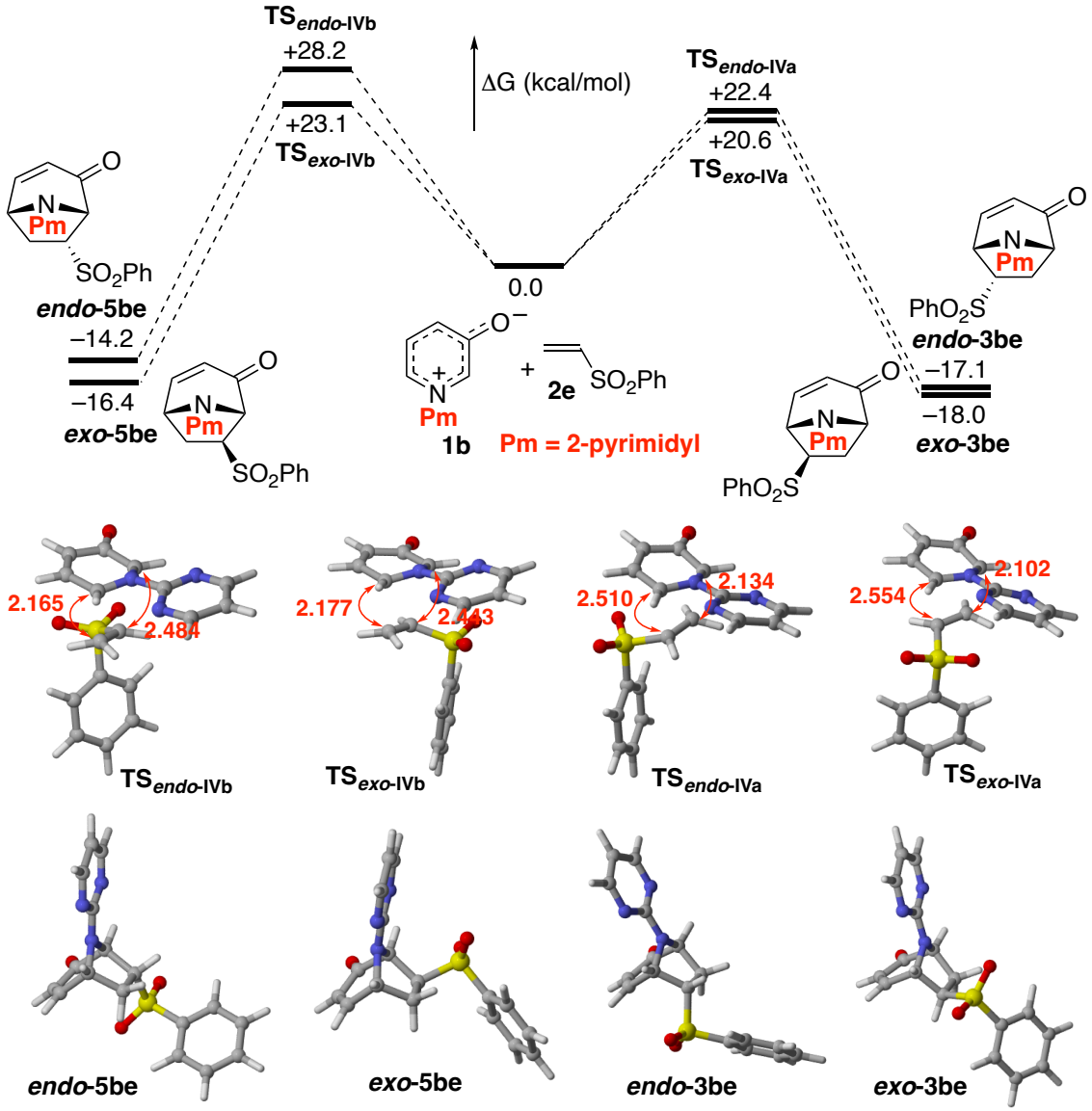

SMD (toluene) M06-2X/6-311+G(2df,2p)//SMD (toluene) ωB97X-D/6-31G(d)

Figure 6. Energy profiles for the (5+2) cycloaddition of betaine **1b** and phenyl vinyl sulfone (**2e**) with relative Gibbs energies (298 K, 1 atm).

(5+6) and (5+4) cycloadditions of 1-(2-pyrimidyl)-3-oxidopyridinium. Katritzky *et al.* reported that the cycloaddition of betaine **1c** with 6,6-dimethylfulvene as

a 6π component at 20 °C in diethyl ether afforded the (5+6) cycloadduct in 31% yield.[7] Later, Radhakrishnan *et al.* reported the cycloaddition of betaines **1b** and **1c** with various pentafulvenes in tetrahydrofuran (THF) between 0 °C and room temperature over 6 h, and the yields were significantly improved (63–72%).[8] We also revisited the cycloaddition of **1b** with pentafulvenes. At the outset, a mixture of **1b**-H and 6,6-diphenylfulvene (**6a**, 1 equiv) was treated with triethylamine (1 equiv) in THF at room temperature for 6 h; however, the reaction was sluggish, generating the expected product in a low yield. Thus, the reaction was repeated in THF under reflux for 23 h, affording **7ba** in 55% yield along with trace amounts of inseparable byproduct(s) as shown in Scheme 4. The reaction of **1b**-H with 6,6-dimethylfulvene (**6b**) was conducted in a similar manner to afford **7bb** along with an inseparable minor product in a 1.5:1 ratio. The spectral data for **7ba** and **7bb** were in good accordance with those previously reported.[8]

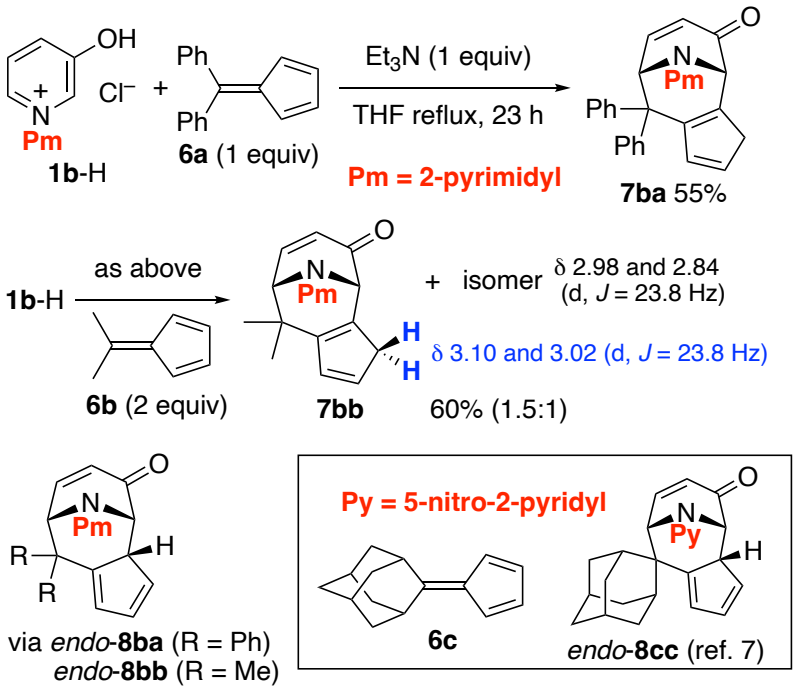

Scheme 4. Reaction of betaine **1b** with pentafulvenes **6a** and **6b**.

Cycloadducts **7ba** and **7bb** were formed via 1,5-H shift from the initial products *endo*-**8ba** and *endo*-**8bb**, respectively. Radhakrishnan *et al.* obtained *endo*-**8cc** through the reaction of betaine **1c** with adamantylidenefulvene **6c**, and its structure was unambiguously confirmed using single X-ray crystallography (Scheme 4).[8] The minor product formed in the reaction of **1b** with **6b** might be a double-bond positional isomer caused by the 1,5-H shift in the cyclopentadiene moiety. The methylene protons of the minor product were observed at δ 2.98 and 2.84 ppm as a pair of doublets with the coupling constant J = 23.8 Hz, while those of **7bb** were observed at δ 3.10 and 3.02 ppm

as a pair of doublets with the coupling constant J = 23.8 Hz. To gain insight into the formation mechanism of **7bb**, DFT calculations were performed (Figure 7a). The *exo*-mode (5+6) cycloaddition of **1b** with **6b** proceeds via **TS*exo*-V** with a high activation barrier ($\Delta G^{\ddagger}$ = +31.6 kcal/mol), suggesting that this process is kinetically infeasible under the experimental conditions. In addition, the formation of *exo*-**8bb** from **1b** and **6b** is only slightly exergonic (–1.5 kcal/mol). We then examined *endo*-mode cycloaddition to determin the corresponding transition state (**TS*endo*-V**). To confirm the connectivity of the *endo*-mode cycloaddition step, intrinsic reaction coordinate (IRC) calculations from **TS*endo*-V** and subsequent optimization of the resultant product geometry were performed, generating the (5+4) cycloadduct (***endo*-9bb**) rather than the expected (5+6) cycloadduct (***endo*-8bb**). Further inspection of the potential energy surface connecting ***endo*-9bb** and ***endo*-8bb** led to the identification of an alternative transition state (**TS$_{VI}$**). Both transition states **TS*endo*-V** and **TSVI** ($\Delta G^{\ddagger}$ = +23.7 and +22.7 kcal/mol, respectively) were located much lower than **TS*exo*-V**, and the formations of *endo*-**8bb** and *endo*-**9bb** are kinetically feasible. However, the formation of *endo*-**9bb** form **1b** and **6b** is endergonic (+4.1 kcal/mol), while that of *endo*-**8bb** is exergonic (–8.8 kcal/mol). Accordingly, the *endo*-

mode cycloaddition of **1b** with **6b** ultimately affords *endo*-**8bb**. The final 1,5-H shift from *endo*-**8bb** proceeds via **TSVII** with a reasonable activation barrier ($\Delta G^{\ddagger}$ = +23.6 kcal/mol) to afford **7bb**. The formation of **7bb** from **1b**+**6b** is exergonic by 11.0 kcal/mol.

A related *endo*-mode (5+6) cycloaddition of oxidopyrylium betaine with pentafulvenes was previously investigated using DFT calculations; however, no information on the involvement of (5+4) cycloaddition was provided.[14] Thus, we reinvestigated the *endo*-mode cycloaddition of oxidopyrylium betaine **s3** with **6b** and the results are shown in Figure S7 (Supporting Information). The first transition state (**TS*endo*-sIV**) was located +15.8 kcal/mol above **s3** + **6b**, showing the higher reactivity of **s3** compared with **1b**. In contrast to the case of **1b**, the IRC calculation led to the formation of (5+6) cycloadduct *endo*-**s5**, although transition states **TS*endo*-V** (Figure 7a) and **TS*endo*-sIV** are very similar; the C(2)–C(a) distances are approximately 2.1 Å, and the C(4)–C(b) and C(6)–C(c) distances are very close (ca. 2.9 Å). Nevertheless, the C(4)–C(b) distance is slightly shorter than the C(6)–C(c) distance in **TS*endo*-V** whereas the latter is slightly shorter than the former in **TS*endo*-sIV**. Although this difference is reflected in the IRC calculation results, both the (5+4) and (5+6) cycloadditions can proceed after passing

ambimodal TSs (**TS*endo*-V** and **TS*endo*-sIV**). This type of post-TS bifurcation has been reported for the (5+2) vs. (5+4) cycloaddition of oxidopyrylium betaine with 1,3-butadiene, and ambimodal (6+4) cycloaddition of tropone with 6,6-dimethylfulvene.[15] The potential energy surface derived from **TS*endo*-V** by modulating the C(4)–C(b) and C(6)–C(c) distances (Figure 7b) shows that reaction pathway bifurcation occurrs as the C(2)–C(a) distance shortened after passing **TS*endo*-V** (Pt7). In path A, the C(6)–C(c) bond is formed to produce *endo*-**8bb**, whereas the C(4)–C(b) bond is formed in path B, leading to *endo*-**9bb**. Although both *endo*-**9bb** and *endo*-**8bb** can be produced by this pathway bifurcation, (5+4) cycloadduct *endo*-**9bb** subsequently undergoes isomerization to afford more thermodynamically favored *endo*-**8bb** via **TS$_{VI}$** (path C). A similar analysis for the cycloaddition of **s3** and **6b** is shown in Figure S7. Moreover, DFT analysis suggests that the reaction of 1-methyl-3-oxidopyridinium **1a** with **6b** is infeasible as the activation barriers for cycloaddition, leading to the (5+6) cycloadduct and subsequent isomerization to the (5+4) cycloadduct, are too high to overcome under experimental conditions ($\Delta G^{\ddagger}$ = +31.3 and +32.9 kcal/mol, respectively), as shown in Figure S8 (Supporting Information). Therefore, the *N*-substituents of oxidopyridinium betaines also play an

important role in the (5+6) cycloaddition with pentafulvenes.

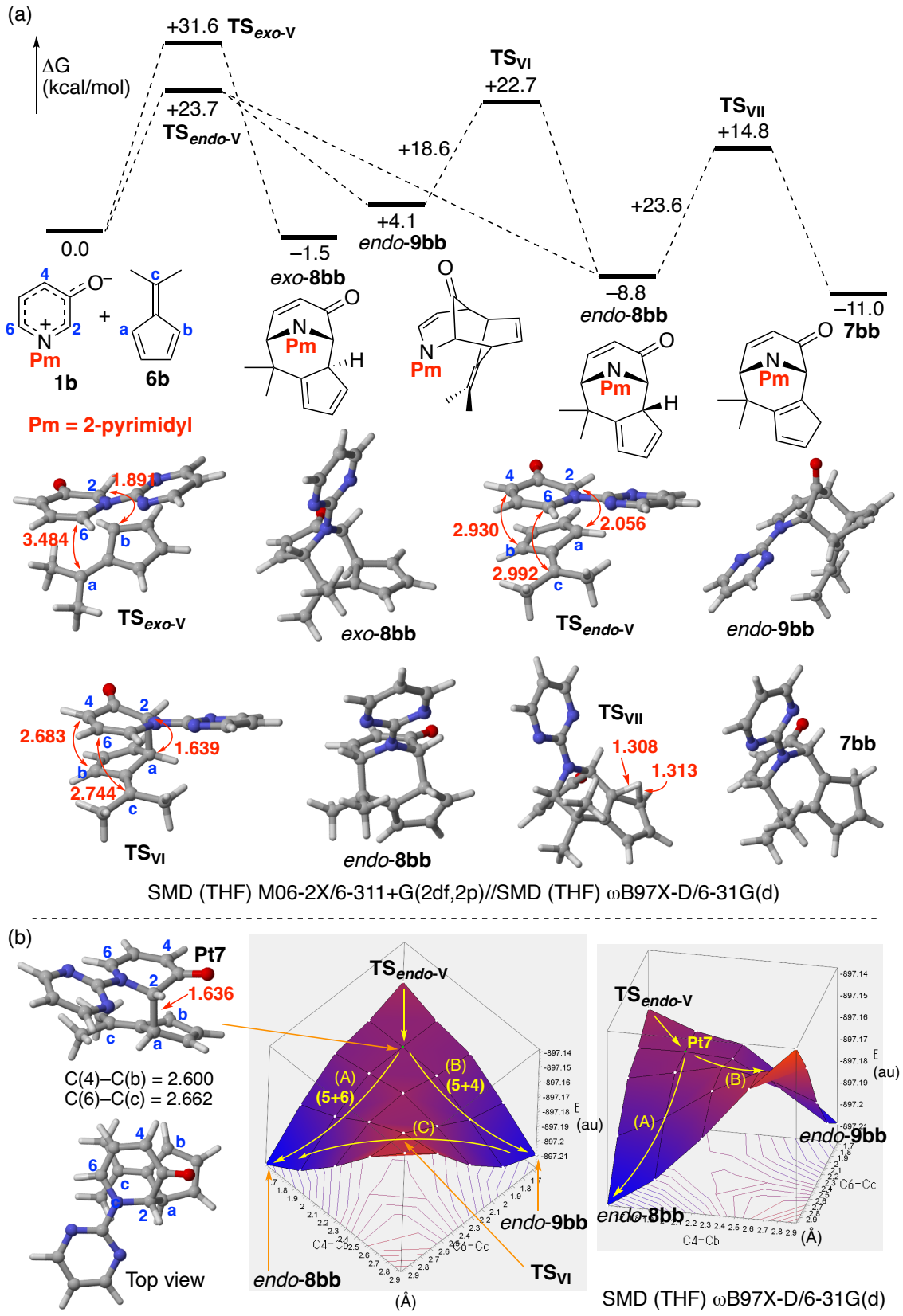

Figure 7. (a) Energy profiles for the cycloaddition of betaine **1b** and 6,6-dimethylfulvene

(**6b**) with relative Gibbs energies (298 K, 1 atm), and (b) relaxed potential energy surface derived from **TS*endo*-V** by modulating the C4–Cb and C6–Cc distances (E: electronic energy without zero-point energy correction). Interatomic distances are given in Å.

It was found that the 1,5-H shift of initial (5+6) cycloadduct *endo*-**8bb** leading to major product **7bb** is facile because the activation barrier ($\Delta G^{\ddagger}$ = +23.6 kcal/mol) can be overcome under experimental conditions. In addition, **7bb** is 2.2 kcal/mol more stable than *endo*-**8bb**. In contrast, an alternative 1,5-H shift from *endo*-**8bb** to *endo*-**10bb** is less efficient because of the higher activation barrier ($\Delta G^{\ddagger}$ = +25.2 kcal/mol), and *endo*-**10bb** is 6.0 kcal/mol less stable than *endo*-**8bb** (path B, Figure 8). Further inspection of the possible 1,5-H shift pathways from **7bb** shows that the interconversion between **7bb** and **12bb** occurs via **11bb** through sequential 1,5-H shifts (paths C and D). The activation barriers ($\Delta G^{\ddagger}$ = +22.8–24.3 kcal/mol) are sufficiently low to overcome under experimental conditions, and **12bb** is only 0.5 kcal/mol less stable than **7bb**. Accordingly, the minor product was tentatively identified as **12bb**.

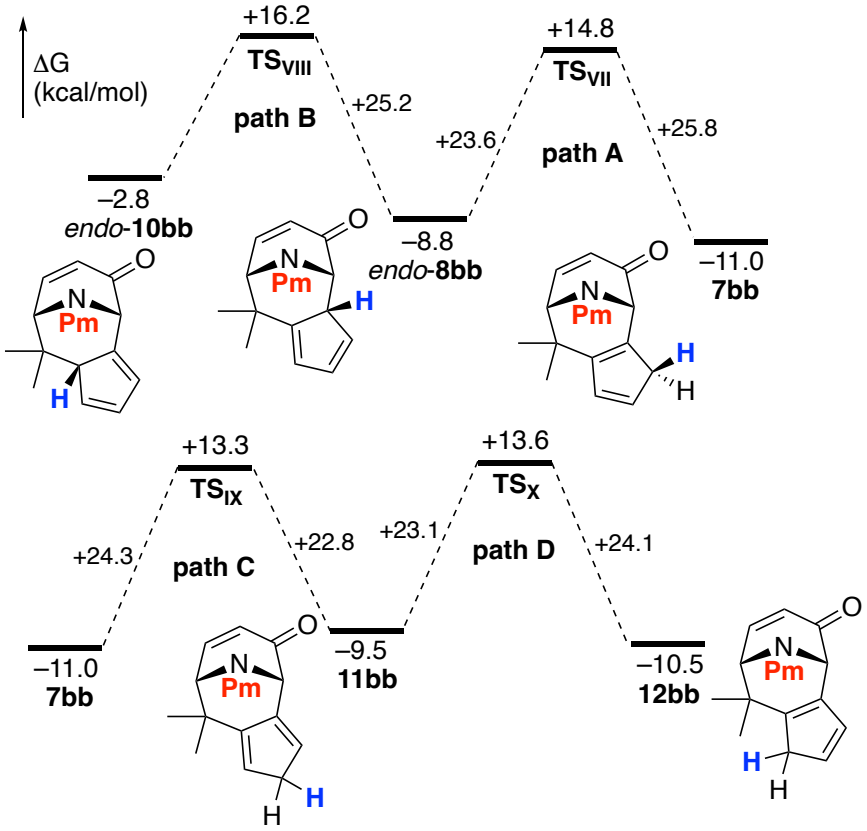

SMD (THF) M06-2X/6-311+G(2df,2p)//SMD (THF) ωB97X-D/6-31G(d)

Figure 8. Energy profiles for 1,5-H shifts from *endo*-**8bb** with relative Gibbs energies (298 K, 1 atm).

The (5+4) cycloaddition of 1-azinyl-3-oxidopyridinium betaines with 1,3-butadienes was reported by the Katritzky group,[6] and later Krenske, Harmata, and coworkers demonstrated that a similar (5+4) cycloaddition efficiently took place with the 1-methyl-3-oxidopyridinium betaine bearing an ester substituent at the 5-position.[16] The (5+4) cycloaddition of betaine **1b** was also observed when in the presence of

triethylamine (2 equiv), **1b**-H and 2,3-dimethyl-1,3-butadiene (**13**, 5 equiv) were heated in DCE at 60 °C (Scheme 5). As a result, the expected product **14** was obtained, albeit in a moderate yield (46%). Trace amounts of the (5+2) cycloadduct were also detected in the crude reaction mixture.

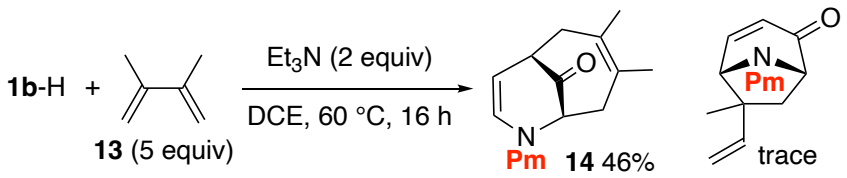

Scheme 5. Reaction of betaine **1b** with 2,3-dimethyl-1,3-butadiene (**13**).

Conclusions

We conducted a combined theoretical and experimental study on the cycloaddition of oxidopyridinium betaines with different *N*-substituents. Accordingly, we found that 1-(2-pyrimidyl)-3-oxidopyridinium betaine shows favorable reactivity and stereoselectivity toward various dipolarophiles such as *N*-methylmaleimide, acenaphthylene, dimethyl maleate, dimethyl acetylenedicarboxylate, phenyl vinyl sulfone, and styrene. Moreover, theoretical analyses of the (5+6) cycloaddition of 1-(2-pyrimidyl)-3-oxidopyridinium and

related oxidopyrylium betaines with 6,6-dimethylpentafulvene suggested the possibility of post-TS bifurcation, leading to (5+6) and (5+4) cycloadducts, although the latter was not experimentally observed. A related (5+4) cycloaddition was observed in the reaction of 1-(2-pyrimidyl)-3-oxidopyridinium with 2,3-dimethyl-1,3-butadiene.

Experimental Section

General Information. All air- and moisture sensitive reactions were performed under an argon atmosphere in dried glassware. Analytical thin layer chromatography was performed using 0.25 mm silica gel plate (Merck TLC Silica gel 60 F_{254}). Column chromatography was performed on silica gel (Cica silica gel 60N) with eluents specified below. NMR spectra were recorded for samples in $CDCl_3$ solutions at 25 °C. ^1H NMR chemical shifts are reported in terms of chemical shift (δ, ppm) relative to the singlet at δ 0.00 ppm for TMS. ^{13}C NMR spectra were fully decoupled and are reported in terms of chemical shift (δ, ppm) relative to the triplet at δ 77.0 ppm for $CDCl_3$. Splitting patterns are designated as follows: s, singlet; d, doublet; t, triplet; q, quartet; quint, quintet; sext, sextet; sept, septet; m, multiplet; br, broad. Coupling constants are reported in Hz. High

resolution mass spectra (HRMS) were obtained on a DART-TOF or ESI-TOF mass spectrometer. Pyridin-3-ol, 5-chloropyridin-3-ol, iodomethane, 2-chloropyrimidine, 2-chloro-5-nitropyridine and dipolarophiles (**2a**−**f**, **6a,b**, and **13**) were purchased and used as received. The reactions requiring heating were performed using PERSONAL SYNTHESIZER (EYELA ChemiStation PPS-CTRL1). Known pyridinium salts **1b**-H and **1c**-H were prepared according to the literature.[8,12]

Computational Methods

The Gaussian 16 program package was used for all calculations.[17] The potential energy surface explorations and full geometry optimizations of the stationary points and transition states were performed using a long-range corrected hybrid functional with damped dispersion corrections, ωB97X-D,[18] and the 6-31G(d)[19] basis sets. The vibrational frequencies and the thermal correction to Gibbs free energy (TCGFE), including the zero-point energy, were calculated at the same level of theory. The obtained structures were characterized by the number of imaginary frequencies (one or zero for the transition and ground states, respectively). Additionally, the connectivity of each step was

also confirmed using intrinsic reaction coordinate (IRC)[20] calculations from the transition states, followed by the optimization of the resultant geometries. Single-point energies for geometries obtained using the above method were calculated using Truhlar's M06-2X functional[21] with the 6-311+G(2df,2p) basis sets.[22] This method has been reported to give good results for Diels–Alder reaction.[23] To examine the solvent effect, the potential energy surface explorations, geometry optimizations, and single-point energy calculations were performed using the SMD model[24] with experimentally used solvents. The obtained results are summarized in Table S1 (Supporting Information). CYLview (Ver. 1.0b)[25] was used to visualize the optimized structures. NCI analysis[11] was performed using the Multiwfn 3.7 program[26] and the results were visualized using the VMD for WIN64 (Ver. 1.9.4a53) program.[27]

Synthesis of 3-chloro-5-hydroxy-1-(pyrimidin-2-yl)pyridin-1-ium chloride (1b(Cl)-H).

According to the literature procedure,[12] 5-chloropyridin-3-ol (647.6 mg, 5.00 mmol) and 2-chloropyrimidine (573.0 mg, 5.00 mmol) were stirred at 120 °C in chlorobenzene (5

mL) for 14 h. After cooled to room temperature, insoluble materials were filtered off and washed with acetone. The filtrate was concentrated in vacuo, and **1b(Cl)-H)** was precipitated from hot ethanol/hexane (three times, 911.6 mg, 75%) as a brown solids (mp 213.0–213.7 °C): ^{1}H NMR (400 MHz, acetone-d_6, 25 °C): δ 9.64–9.59 (m, 2H), 9.22 (d, 2H, J = 5.0 Hz), 8.54 (s, 1H), 7.99 (t, 1H, J = 5.0 Hz), 6.07 (s, 1H), 5.54 (s, 1H), 5.28 (s, 1H), 3.56 (d, 1H, J = 7.6 Hz), 3.36 (d, 1H, J = 7.6 Hz), 3.03 (s, 3H); ^{13}C{^{1}H} NMR (100 MHz, acetone-d_6, 25 °C): δ 160.7, 158.0, 154.5, 135.3, 134.7, 130.7, 128.5, 124.6; HRMS (DART) *m/z* [betaine dimer+H]$^{+}$ calcd for $C_{18}H_{13}Cl_2N_6O_2$ 415.0477, found 415.0484.

Synthesis of (3a*S,4*S**,8*S**,8a*R**)-2,9-dimethyl-3a,4,8,8a-tetrahydro-4,8-epiminocyclohepta[*c*]pyrrole-1,3,5(2*H*)-trione (*exo*-3aa).**

To a solution of 3-hydroxypyridine (95.1 mg, 1.00 mmol) in dry acetone (0.5 mL) was added iodomethane (0.187 mL, 3.00 mmol) at room temperature. The reaction mixture was stirred at 50 °C for 3 h under an argon atmosphere. The solvent was evaporated *in vacuo*, and the obtained crude product was diluted with dry toluene (4.0 mL). To the obtained mixture was added *N*-methylmaleimide (111.1 mg, 1.00 mmol) and triethylamine (0.278 mL, 2.00 mmol). The reaction mixture was stirred at 110 °C under

an argon atmosphere for 16 h. After adding H_2O (6 mL), aqueous phase was extracted with AcOEt (3×10 mL). The combined organic extract was dried over anhydrous Na_2SO_4. The solvents were evaporated *in vacuo*, and the obtained crude product was purified by silica gel column chromatography (hexane/AcOEt, 2:1~1:1) to afford ***exo*-3aa** (170.5 mg, 77%) as a yellow solid (mp 163.3–164.0 °C). Following spectral data are in good accordance with those previously reported:[4a] ^{1}H NMR (400 MHz, $CDCl_3$, 25 °C): δ 7.02 (dd, 1H, J = 9.8, 5.0 Hz), 6.12 (dd, 1H, J = 9.8, 1.8 Hz), 4.03 (d, 1H, J = 4.4 Hz), 3.77 (s, 1H), 3.28 (d, 1H, J = 7.4 Hz), 3.08 (d, 1H, J = 7.4 Hz), 3.04 (s, 3H), 2.41 (s, 3H); ^{13}C{^{1}H} NMR (100 MHz, $CDCl_3$, 25 °C): δ 194.8, 176.0, 175.8, 146.1, 127.5, 72.0, 61.0, 51.1, 46.1, 33.6, 25.1.

Synthesis of (3a*S,4*S**,8*S**,8a*R**)-2-methyl-9-(pyrimidin-2-yl)-3a,4,8,8a-tetrahydro-4,8-epiminocyclohepta[*c*]pyrrole-1,3,5(2*H*)-trione (*exo*-3ba) [General Procedure A]**.

A mixture of pyridinium salt **1b**-H (62.8 mg, 0.300 mmol), *N*-methylmaleimide (33.3 mg, 0.300 mmol) and triethylamine (0.0835 mL, 0.600 mmol) in dry toluene (1 mL) was stirred at 110 °C under an argon atmosphere for 16 h. To the obtained mixture was added

H_2O (10 mL) at room temperature, and aqueous phase was extracted with AcOEt (3×10 mL). The combined organic extract was dried over anhydrous Na_2SO_4. The solvents were evaporated *in vacuo*, and the obtained crude product was purified by silica gel column chromatography (hexane/AcOEt, 2:1~1:1) to afford ***exo/endo*-3ba** (65.9 mg, 77%, *exo*/*endo* >10:1) as a brown solid (mp 205.7–207.5 °C). Analytical data for ***exo*-3ba**: ^{1}H NMR (400 MHz, $CDCl_3$, 25 °C): δ 8.36 (d, 2H, *J* = 4.8 Hz), 7.43 (dd, 1H, *J* = 10.0, 5.2 Hz), 6.73 (t, 1H, *J* = 4.8 Hz), 5.99 (dd, 1H, *J* = 9.8, 1.4 Hz), 5.55 (d, 1H, *J* = 5.2 Hz), 5.33 (s, 1H), 3.42 (d, 1H, *J* = 7.2 Hz), 3.31 (d, 1H, *J* = 7.2 Hz), 3.00 (s, 3H); $^{13}C\{^1H\}$ NMR (100 MHz, $CDCl_3$, 25 °C): δ 192.8, 175.2, 175.0, 161.2, 158.0, 151.3, 128.4, 113.7, 67.7, 57.4, 50.4, 46.0, 25.5; HRMS (ESI) *m/z* $[M+Na]^+$ calcd for $C_{14}H_{12}N_4NaO_3$ 307.0807, found 307.0836.

Scale-up procedure – Synthesis of (3a*S,4*S**,8*S**,8a*R**)-2-methyl-9-(pyrimidin-2-yl)-3a,4,8,8a-tetrahydro-4,8-epiminocyclohepta[*c*]pyrrole-1,3,5(2*H*)-trione (*exo*-3ba)**.

A mixture of pyridinium salt **1b**-H (209.5 mg, 0.999 mmol), *N*-methylmaleimide (111.3 mg, 1.00 mmol) and triethylamine (0.278 mL, 2.00 mmol) in dry toluene (2 mL) was

stirred at 110 °C under an argon atmosphere for 16 h. To the obtained mixture was added H_2O (10 mL) at room temperature, and aqueous phase was extracted with AcOEt (3×20 mL). The combined organic extract was dried over anhydrous Na_2SO_4. The solvents were evaporated *in vacuo*, and the obtained crude product was purified by recrystallization (hexane/$CHCl_3$) to afford ***exo/endo*-3ba** (199.1 mg, 70%, *exo*/*endo* >10:1) as a brown solid.

Synthesis of 7-chloro-2-methyl-9-(pyrimidin-2-yl)-3a,4,8,8a-tetrahydro-4,8-epiminocyclohepta[*c*]pyrrole-1,3,5(2*H*)-trione (*exo/endo*-3b(Cl)a).

This compound was synthesized according to General Procedure A, except for the use of **1b(Cl)**-H (73.1 mg, 0.300 mmol). Purification by silica gel column chromatography (hexane/AcOEt, 3:1~2:1~1:1) to afford of ***exo*-3b(Cl)a** (85.2 mg, 89%) as a colorless solid (mp 212.6–213.7 °C) along with ***exo*-3b(Cl)a** (<4.7 mg, <5%).

Analytical data for ***exo*-3b(Cl)a**: ^{1}H NMR (400 MHz, $CDCl_3$, 25 °C): δ 8.41 (d, 2H, J = 4.8 Hz), 6.81 (t, 1H, J = 4.8 Hz), 6.07 (s, 1H), 5.54 (s, 1H), 5.28 (s, 1H), 3.56 (d, 1H, J = 7.6 Hz), 3.36 (d, 1H, J = 7.6 Hz), 3.03 (s, 3H); ^{13}C{^{1}H} NMR (100 MHz, $CDCl_3$, 25 °C): δ 190.7, 174.5, 174.3, 160.9, 158.9, 158.1, 125.8, 114.4, 66.5, 64.3, 50.0, 46.5, 25.7;

HRMS (DART) *m/z* $[M+H]^+$ calcd for $C_{14}H_{12}ClN_4O_3$ 319.0598, found 319.0627.

Analytical data for ***endo*-3b(Cl)a**: Because of the low yield, only ^1H NMR spectrum was recorded. ^1H NMR (400 MHz, $CDCl_3$, 25 °C): δ 8.42 (d, 2H, J = 4.8 Hz), 6.81 (t, 1H, J = 4.8 Hz), 6.11 (s, 1H), 5.71–5.68 (m, 1H), 5.42–5.38 (m, 1H), 4.12–4.05 (m, 2H), 2.97 (s, 3H).

Synthesis of 12-(pyrimidin-2-yl)-6b,7,11,11a-tetrahydro-8*H*-7,11-epiminocyclohepta[*a*]acenaphthylen-8-one (3bb) [General Procedure B].

A mixture of pyridinium salt **1b**-H (62.8 mg, 0.300 mmol), acenaphthylene (136.8 mg, 0.900 mmol) and triethylamine (0.0835 mL, 0.600 mmol) in dry xylene (1 mL) was stirred at 130 °C under an argon atmosphere for 16 h. To the obtained mixture was added H_2O (5 mL) at room temperature, and aqueous phase was extracted with AcOEt (3×10 mL). The combined organic extract was dried over anhydrous Na_2SO_4. The solvents were evaporated *in vacuo*, and the obtained crude product was purified by silica gel column chromatography (hexane/AcOEt, 3:1~2:1) to afford ***endo*-3bb** (9.9 mg, 10%) as a yellow solid. Further elution (hexane/AcOEt, 2:1~1:1) afforded a mixture of ***endo/exo*-3bb** (26.0 mg, 27%; *endo*/*exo* 1:4). Further elution (hexane/AcOEt, 1:1) afforded ***exo*-3bb** (29.3 mg,

30%) as a yellow solid (mp 186.8–188.1 °C).

Analytical data for ***exo*-3bb**: ^{1}H NMR (400 MHz, $CDCl_3$, 25 °C): δ 8.17 (d, 2H, *J* = 4.8 Hz), 7.68–7.66 (m, 2H), 7.63 (dd, 1H, *J* = 9.6, 4.8 Hz), 7.55–7.46 (m, 4H), 6.50 (t, 1H, *J* = 4.8 Hz), 6.03 (dd, 1H, *J* = 9.6, 1.2 Hz), 5.41 (d, 1H, *J* = 5.2 Hz), 5.17 (s, 1H), 4.34 (d, 1H, *J* = 6.4 Hz), 4.23 (d, 1H, *J* = 6.4 Hz); ^{13}C{^{1}H} NMR (100 MHz, $CDCl_3$, 25 °C): δ 196.2, 162.0, 157.5, 153.6, 143.4, 143.2, 140.0, 130.9, 128.4, 128.1, 127.4, 123.8, 123.7, 120.4, 119.6, 112.3, 71.8, 60.7, 54.5, 50.2; HRMS (ESI) *m/z* $[M+Na]^+$ calcd for $C_{21}H_{15}N_3NaO$ 348.1113, found 348.1134.

Analytical data for ***endo*-3bb**: Because of the low yield, only ^{1}H NMR spectrum was recorded. ^{1}H NMR (400 MHz, $CDCl_3$, 25 °C): δ 8.38 (d, 2H, *J* = 4.8 Hz), 7.63 (t, 2H, *J* = 8.4 Hz), 7.45 (ddd, 2H, *J* = 8.0, 6.8, 1.8 Hz), 7.38 (d, 1H, *J* = 6.8 Hz), 7.29 (d, 1H, *J* = 7.2 Hz), 6.67 (t, 1H, *J* = 4.8 Hz), 6.66 (dd, 1H, *J* = 9.6, 4.8 Hz), 5.74 (dd, 1H, *J* = 6.8, 4.8 Hz), 5.58 (d, 1H, *J* = 8.8 Hz), 5.29 (dd, 1H, *J* = 9.6, 1.2 Hz), 4.93 (dd, 1H, *J* = 8.8, 7.6 Hz), 4.83 (dd, 1H, *J* = 8.0, 6.8 Hz).

Synthesis of 10-chloro-12-(pyrimidin-2-yl)-6b,7,11,11a-tetrahydro-8*H*-7,11-epiminocyclohepta[*a*]acenaphthylen-8-one (*exo/endo*-3b(Cl)b).

This compound was synthesized according to General Procedure B, except for the use of **1b(Cl)**-H (73.1 mg, 0.300 mmol). Purification by silica gel column chromatography (hexane/AcOEt, 5:1~3:1~2:1) to afford of ***exo*-3b(Cl)b** (65.4 mg, 61%) as an orange solid (mp 245.2– 246.2°C). Further elution afforded ***eno*-3b(Cl)b** (13.4 mg, 12%, *exo*/*endo* 1:20).

Analytical data for ***exo*-3b(Cl)b**: ^{1}H NMR (400 MHz, $CDCl_3$, 25 °C): δ 8.24 (d, 2H, *J* = 4.8 Hz), 7.71–7.67 (m, 2H), 7.57–7.51 (m, 4H), 6.59 (t, 1H, *J* = 4.8 Hz), 6.12 (s, 1H), 5.42 (s, 1H), 5.13 (s, 1H), 4.47 (d, 1H, *J* = 7.2 Hz), 4.29 (d, 1H, *J* = 7.2 Hz); ^{13}C{^{1}H} NMR (100 MHz, $CDCl_3$, 25 °C): δ 194.0, 161.8, 161.1, 157.8, 142.9, 142.6, 139.9, 131.0, 128.5, 128.2, 124.9, 124.1, 124.0, 120.4, 119.9, 113.2, 70.6, 67.8, 54.5, 50.9; HRMS (DART) *m/z* $[M+H]^+$ calcd for $C_{21}H_{15}ClN_3O$ 360.0904, found 360.0912.

Analytical data for ***endo*-3b(Cl)b**: ^{1}H NMR (400 MHz, $CDCl_3$, 25 °C): δ 8.42 (d, 2H, *J* = 4.8 Hz), 7.67 (t, 1H, *J* = 8.8 Hz), 7.63 (d, 1H, *J* = 8.4 Hz), 7.49–7.42 (m, 3H), 7.28 (d, 1H, *J* = 6.8 Hz), 6.73 (t, 1H, *J* = 4.8 Hz), 5.78 (d, 1H, *J* = 6.8 Hz), 5.53 (d, 1H, *J* = 8.0 Hz), 4.99–4.92 (m, 2H); ^{13}C{^{1}H} NMR (100 MHz, $CDCl_3$, 25 °C): δ 192.8, 161.4, 159.0, 158.1, 140.8, 139.6, 138.9, 131.4, 128.0, 127.3, 127.1, 124.4, 124.0, 122.20, 122.17,

113.3, 66.6, 64.4, 53.2, 50.4.

Synthesis of dimethyl (1*S,5*S**,6*S**,7*R**)-4-oxo-8-(pyrimidin-2-yl)-8-azabicyclo[3.2.1]oct-2-ene-6,7-dicarboxylate (*exo*-3bc) [General Procedure C]**.

A mixture of pyridinium salt **1b**-H (62.7 mg, 0.300 mmol) and triethylamine (0.0501 mL, 0.360 mmol) in dry toluene (1 mL) was stirred at room temperature for 0.5 h. After adding dimethyl maleate (0.0751 mL, 0.600 mmol) at room temperature, the reaction mixture was stirred at 110 °C under an argon atmosphere for 16 h. To the obtained mixture was added H_2O (5 mL) at room temperature, and aqueous phase was extracted with AcOEt (3×10 mL). The combined organic extract was dried over anhydrous Na_2SO_4. The solvents were evaporated *in vacuo*, and the obtained crude product was purified by silica gel column chromatography (hexane/AcOEt, 1.5:1~1:2) to afford an inseparable mixture of ***endo*-3bc** and *trans*-isomers (26.2 mg, 28%, *endo*/*trans* 3:1). Further elution afforded ***exo*-3bc** (37.8 mg, 40%) as a yellow solid (mp 144.0–144.6 °C).

Analytical data for ***exo*-3bc**: ^{1}H NMR (400 MHz, $CDCl_3$, 25 °C): δ 8.35 (d, 2H, J = 4.4 Hz), 7.36 (dd, 1H, J = 9.8, 5.0 Hz), 6.67 (t, 1H, J = 4.8 Hz), 5.96 (dd, 1H, J = 9.6, 1.2 Hz), 5.61 (d, 1H, J = 5.2 Hz), 5.52 (s, 1H), 3.73 (s, 3H), 3.69 (s, 3H), 3.46 (d, 1H, J = 9.6

Hz), 3.33 (d, 1H, J = 9.2 Hz); $^{13}C\{^{1}H\}$ NMR (100 MHz, $CDCl_3$, 25 °C): δ 194.5, 170.4, 170.3, 160.6, 157.8, 150.9, 128.0, 112.6, 66.5, 57.7, 52.5, 52.4, 49.2, 46.5; HRMS (ESI) *m/z* $[M+Na]^+$ calcd for $C_{15}H_{15}N_3NaO_5$ 340.0909, found 340.0893.

Synthesis of dimethyl 4-oxo-8-(pyrimidin-2-yl)-8-azabicyclo[3.2.1]octa-2,6-diene-6,7-dicarboxylate (3bd).

This compound was synthesized according to General Procedure C. Purification by silica gel column chromatography (hexane/AcOEt, 3:1~1:1) to afford **3bd** (68.1 mg, 72%) as a yellow oil: ^{1}H NMR (400 MHz, $CDCl_3$, 25 °C): δ 8.40 (d, 2H, J = 4.4 Hz), 7.45 (dd, 1H, J = 9.6, 4.4 Hz), 6.76 (t, 1H, J = 4.8 Hz), 5.71 (d, 1H, J = 4.0 Hz), 5.70 (s, 1H), 5.55 (dd, 1H, J = 9.6, 1.6 Hz), 3.88 (s, 3H), 3.86 (s, 3H); $^{13}C\{^{1}H\}$ NMR (100 MHz, $CDCl_3$, 25 °C): δ 189.1, 162.4, 162.0, 160.3, 158.1, 150.2, 147.5, 139.6, 124.5, 113.4, 73.4, 61.9, 52.73, 52.71; HRMS (ESI) *m/z* $[M+Na]^+$ calcd for $C_{15}H_{13}N_3NaO_5$ 338.0753, found 338.0772.

Preparation of dimer *exo*-4a from 1b-H.

A mixture of pyridinium salt **1b**-H (104,.84 mg, 0.500 mmol) and triethylamine (0.0835 mL, 0.600 mmol) in dry 1,2-dichloroethane (1 mL) was stirred at room temperature under an argon atmosphere for 0.5 h. Insoluble materials were filtered off, and the filtrate was

washed with H_2O (2×10 mL). The organic extract was dried over anhydrous Na_2SO_4. The solvents were evaporated *in vacuo* to afford crude ***exo*-4a** containing 1,2-dichloroethane (75.5 mg, ca. 87%) as a brown solid: ^{1}H NMR (400 MHz, $CDCl_3$, 25 °C): δ 8.47 (br s, 2H), 8.24 (br s, 1H), 7.83 (br s, 1H), 7.46 (d, 1H, *J* = 8.0 Hz), 7.28 (dd, 1H, *J* = 10.0, 5.6 Hz), 6.80 (t, 1H, *J* = 4.8 Hz), 6.51 (t, 1H, *J* = 4.8 Hz), 6.42–6.39 (m, 1H), 6.28 (d, 1H, *J* = 9.6 Hz), 6.13 (dt, 1H, *J* = 5.2, 2.5 Hz), 5.23 (t, 1H, *J* = 2.6 Hz), 4.94 (dd, 1H, *J* = 8.0, 6.4 Hz), 3.28 (dt, 1H, *J* = 6.4, 2.4 Hz); ^{13}C{^{1}H} NMR (100 MHz, $CDCl_3$, 25 °C): δ 199.9, 192.1, 160.5, 157.9, 157.2, 157.1, 147.9, 129.8, 129.7, 113.4, 111.8, 97.0, 64.5, 63.8, 56.4, 51.0; HRMS (ESI) *m/z* $[M+Na]^+$ calcd for $C_{18}H_{14}N_6NaO_2$ 369.1076, found 369.1050.

Synthesis of (1*S,5*S**,6*R**)-6-(phenylsulfonyl)-8-(pyrimidin-2-yl)-8-azabicyclo[3.2.1]oct-3-en-2-one (*exo*-3be).**

This compound was synthesized according to General Procedure A. Purification by silica gel column chromatography (hexane/AcOEt, 2:1~1:2) to afford ***exo*-3be** (78.0 mg, 76%) as a yellow solid (mp 190.2–191.1 °C): ^{1}H NMR (400 MHz, $CDCl_3$, 25 °C): δ 8.29 (br s, 2H), 7.93 (d, 2H, *J* = 7.2 Hz), 7.58 (t, 1H, *J* = 7.2 Hz), 7.49 (t, 2H, *J* = 7.2 Hz), 7.32 (dd, 1H, *J* = 9.8, 5.4 Hz), 6.64 (t, 1H, *J* = 4.8 Hz), 5.96 (dd, 1H, *J* = 9.6, 1.2 Hz), 5.69 (d, 1H,

J = 5.2 Hz), 5.04 (d, 1H, *J* = 8.4 Hz), 3.71 (dd, 1H, *J* = 9.2, 4.4 Hz), 2.92 (ddd, 1H, *J* = 14.8, 8.4, 4.4 Hz), 2.20 (dd, 1H, *J* = 14.8, 9.2 Hz); $^{13}C\{^{1}H\}$ NMR (100 MHz, $CDCl_3$, 25 °C): δ 194.9, 160.0, 157.8, 150.1, 136.8, 134.0, 129.2, 129.0, 112.7, 66.3, 63.9, 55.4, 27.3; HRMS (ESI) *m/z* $[M+Na]^+$ calcd for $C_{17}H_{15}N_3NaO_3S$ 364.0732, found 364.0730.

Synthesis of 6-phenyl-8-(pyrimidin-2-yl)-8-azabicyclo[3.2.1]oct-3-en-2-one (*endo*/*exo*-3bf).

This compound was synthesized according to General Procedure B, except for the use of styrene (5 equiv). Purification by silica gel column chromatography (hexane/AcOEt, 3:1~2:1~1:1) to afford inseparable mixture of ***endo*/*exo*-3bf** (63.3 mg, 76%, *endo*/*exo* 6:1) as a yellow paste: ^{1}H NMR (400 MHz, $CDCl_3$, 25 °C): *endo*-isomer δ 8.35 (d, 2H, *J* = 4.8 Hz), 7.36–7.22 (m, 5H), 6.88 (dd, 1H, *J* = 9.6, 5.2 Hz), 6.65 (t, 1H, *J* = 4.8 Hz), 6.02 (dd, 1H, *J* = 9.6, 1.6 Hz), 5.49 (t, 1H, *J* = 5.4 Hz), 5.13 (d, 1H, *J* = 8.8 Hz), 4.06 (dt, 1H, *J* = 9.6, 6.6 Hz), 2.99 (ddd, 1H, *J* = 14.0, 9.6, 8.8 Hz), 2.12 (dd, 1H, *J* = 14.0, 7.2 Hz); *exo*-isomer δ 8.35 (d, 2H, *J* = 4.8 Hz), 7.45 (dd, 1H, *J* = 9.6, 4.8 Hz), 7.36–7.22 (m, 5H), 6.65 (t, 1H, *J* = 4.8 Hz), 5.96 (dd, 1H, *J* = 9.6, 1.0 Hz), 5.21–5.17 (m, 2H), 3.43 (dd, 1H, *J* = 9.0, 3.8 Hz), 2.58 (ddd, 1H, *J* = 14.0, 8.2, 3.9 Hz), 2.43 (dd, 1H, *J* = 14.0, 9.2 Hz);

$^{13}C\{^{1}H\}$ NMR (100 MHz, $CDCl_3$, 25 °C): *endo*-isomer δ 197.0, 161.4, 157.9, 151.7, 138.0, 128.8, 128.5, 128.1, 127.1, 112.3, 64.7, 59.3, 47.1, 30.3; HRMS (ESI) *m/z* $[M+Na]^+$ calcd for $C_{17}H_{15}N_3NaO$ 300.1113, found 300.1117.

Synthesis of 9,9-diphenyl-10-(pyrimidin-2-yl)-3,4,8,9-tetrahydro-5*H*-4,8-epiminocyclopenta[8]annulen-5-one (7ba) [General Procedure D].

A mixture of pyridinium salt **1b**-H (62.9 mg, 0.300 mmol), 6,6-diphenylpentafulvene (69.1 mg, 0.300 mmol) and triethylamine (0.0418 mL, 0.300 mmol) in dry THF (1 mL) was stirred at 70 °C under an argon atmosphere for 23 h. The solvents were evaporated *in vacuo*, and the obtained crude product was purified by silica gel column chromatography (hexane/AcOEt, 6:1) to afford **7ba** containing isomers (66.2 mg, 55%) as a brown oil. Following spectral data are in good accordance with those previously reported:[8] ^{1}H NMR (400 MHz, $CDCl_3$, 25 °C): δ ^{1}H NMR (400 MHz, $CDCl_3$, 25 °C): δ 8.45 (br d, 2H, *J* = 3.6 Hz), 7.62–7.58 (m, 2H), 7.31–7.16 (m, 6H), 7.08–7.05 (m, 2H), 6.72–6.68 (m, 2H), 6.49 (d, 1H, *J* = 5.2 Hz), 6.46 (d, 1H, *J* = 5.2 Hz), 6.05 (dd, 1H, *J* = 10.0, 5.0 Hz), 5.87 (s, 1H), 5.68 (d, 1H, *J* = 10.0 Hz), 3.25 (d, 1H, *J* = 23.8 Hz), 3.13 (d, 1H, *J* = 23.8 Hz); $^{13}C\{^{1}H\}$ NMR (100 MHz, $CDCl_3$, 25 °C): δ 195.1, 161.4, 157.9, 149.0,

145.8, 143.0, 142.5, 134.2, 133.0, 132.7, 129.2, 128.3, 128.2, 128.0, 127.1, 126.3, 125.0, 112.2, 60.1, 56.7, 53.9, 41.1.

Synthesis of 9,9-dimethyl-10-(pyrimidin-2-yl)-3,4,8,9-tetrahydro-5*H*-4,8-epiminocyclopenta[8]annulen-5-one (7bb).

This compound was synthesized according to General Procedure D, except for the use of 6,6-dimethylfulvene (2 equiv). Purification by silica gel column chromatography (hexane/AcOEt, 6:1) to afford **3bb** containing an isomer (50.2 mg, 60%) as a yellow paste. Following spectral data are in good accordance with those previously reported:[8] ^{1}H NMR (400 MHz, $CDCl_3$, 25 °C): δ ^{1}H NMR (400 MHz, $CDCl_3$, 25 °C): δ 8.31 (d, 2H, J = 5.2 Hz), 7.01 (dd, 1H, J = 10.0, 5.0 Hz), 6.53 (t, 1H, J = 4.8 Hz), 6.46–6.31 (m, 2H), 5.90–5.84 (m, 2H), 5.50 (d, 1H, J = 5.6 Hz), 3.10 (d, 1H, J = 23.8 Hz), 3.02 (d, 1H, J = 23.8 Hz), 1.35 (s, 3H), 1.25 (s, 3H); ^{13}C{^{1}H} NMR (100 MHz, $CDCl_3$, 25 °C): δ 195.1, 161.1, 157.7, 147.9, 146.2, 133.6, 131.3, 130.1, 125.6, 110.9, 59.4, 57.0, 41.0, 38.3, 28.9, 23.3.

Synthesis of 3,4-dimethyl-7-(pyrimidin-2-yl)-7-azabicyclo[4.3.1]deca-3,8-dien-10-one (14).

A mixture of pyridinium salt **1b**-H (62.9 mg, 0.300 mmol), 2,3-dimethyl-1,3-butadiene

(0.169 mL, 1.50 mmol) and triethylamine (0.0835 mL, 0.600 mmol) in dry 1,2-dichloroethane (1 mL) was stirred at 60 °C under an argon atmosphere for 16 h. To the obtained mixture was added H_2O (5 mL) at room temperature, and aqueous phase was extracted with AcOEt (3×10 mL). The combined organic extract was dried over anhydrous Na_2SO_4. The solvents were evaporated *in vacuo*, and the obtained crude product was purified by silica gel column chromatography (hexane/AcOEt, 10:1~3:1) to afford **14** (35.3 mg, 46%) as a colorless solid (mp 109.8–111.3 °C): ^{1}H NMR (400 MHz, $CDCl_3$, 25 °C): δ 8.39 (d, 2H, *J* = 4.4 Hz), 7.60 (d, 1H, *J* = 8.4 Hz), 6.68 (t, 1H, *J* = 4.8 Hz), 4.98 (d, 1H, *J* = 7.2 Hz), 4.76 (dd, 1H, *J* = 8.4, 6.0 Hz), 3.15 (dd, 1H, *J* = 14.8, 7.2 Hz), 3.11–3.07 (m, 1H), 2.41 (d, 1H, *J* = 14.4 Hz), 2.36 (dd, 1H, *J* = 14.4, 6.4 Hz), 2.23 (d, 1H, *J* = 14.4 Hz), 1.71 (s, 3H), 1.49 (s, 3H); ^{13}C{^{1}H} NMR (100 MHz, $CDCl_3$, 25 °C): δ 207.3, 157.8, 157.4, 130.2, 127.4, 127.1, 112.3, 100.0, 62.4, 46.6, 39.1, 36.3, 23.3, 22.6; HRMS (DART) *m/z* $[M+H]^+$ calcd for $C_{15}H_{18}N_3O$ 256.1450, found 256.1433.

ASSOCIATED CONTENT

Data Availability Statement

The data underlying this study are available in the published article and its Supporting Information.

Supporting Information

The Supporting Information is available free of charge on the ACS Publication website.

Scheme S1, Figures S1–S6, Table S1, Cartesian coordinates, and ^{1}H and ^{13}C NMR charts (PDF)

AUTHOR INFORMATION

Corresponding Author

*E-mail: yamamoto-yoshi@ps.nagoya-u.ac.jp

Notes

The authors declare no competing financial interest.

ACKNOWLEDGMENTS

This research is partially supported by the Platform Project for Supporting Drug Discovery and Life Science Research (Basis for Supporting Innovative Drug Discovery

and Life Science Research (BINDS) from AMED under Grant Number JP22ama121044) and JSPS KAKENHI (Grant Number JP 22K05110).

REFERENCES

1. (a) Dennis, N.; Katritzky, A. R.; Takeuchi, Y. Synthetic Applications of Heteroaromatic Betaines with Six-Membered Rings. *Angew. Chem. Int. Ed.* **1976**, *15*, 1-60. (b) Katritzky, A. R.; Dennis, N. Cycloaddition Reactions of Heteroaromatic Six-Membered Rings. *Chem. Rev.* **1989**, *89*, 827-861.

2. (a) Jung, M. E.; Longmei, Z.; Tangsheng, P.; Huiyan, Z.; Yan, L.; Jingyu, S. Total Synthesis of Bao Gong Teng A, a Natural Antiglaucoma Compound. *J. Org. Chem.* **1992**, *57*, 3528-3530. (b) Kozikowski, A. P.; Araldi, G. L.; Ball, R. G. Dipolar Cycloaddition Route to Diverse Analogues of Cocaine: The 6- and 7-Substituted 3-Phenyltropanes. *J. Org. Chem.* **1997**, *62*, 503-509. (c) Kozikowski, A. P.; Araldi, G. L.; Prakash, K. R. C.; Zhang, M.; Johnson, K. M. Synthesis and Biological properties of New 2β-Alkyl- and 2β-Aryl-3-(substituted phenyl)tropane Derivatives: Stereochemical Effect of C-3 on Affinity and Selectivity for Neuronal Dopamine and

Serotonin Transporters. *J. Med. Chem.* **1998**, *41*, 4973-4982. (d) Prakash, K. P. C.; Trzcinska, M.; Johnson, K. M.; Kozikowski, A. P. An Enantioselective Synthesis and Biobehavioral Evaluation of 7-Fluoro-3-(*p*-fluorophenyl)-2-propyltropanes. *Bioorg. Med. Chem. Lett.* **2000**, *10*, 1443-1446.

3. According to the IUPAC rules, the cycloaddition symbolism "(*m*+*n*)" is used in this article, although the symbolism "[*m*+*n*]", in which numbers "*m*" and "*n*" show electrons in the interacting units, has been used conventionally for the oxidopyridinium cycloadditions.

4. (a) Xu, H.; Golz, C.; Strohmann, C.; Antonchick, A. P.; Waldmann, H. Enantiodivergent Combination of Natural Product Scaffolds Enabled by Catalytic Enantioselective Cycloaddition. *Angew. Chem. Int. Ed.* **2016**, *55*, 7761-7765. (b) Lowe, R. A.; Taylor, D.; Chibale, K.; Nelson, A.; Marsden, S. P. Synthesis and evaluation of the performance of a small molecule library based on diverse tropane-related scaffolds. *Bioorg. Med. Chem.* **2020**, *28*, 115442.

5. (a) Krüger, S.; Gaich, T. Enantioselective, Protecting-Group-Free Total Synthesis of Sarpagine Alkaloids—A Generalized Approach. *Angew. Chem. Int. Ed.* **2015**, *54*, 315-

317. (b) Krüger, S.; Gaich, T. Total Syntheses of Vellosimine, *N*-Methylvellosimine, and 10-Methoxyvellosimine and Formal Synthesis of 16-Epinormacusine B through a [5+2] Cycloaddition. *Eur. J. Org. Chem.* **2016**, 4893-4899. (c) Gerlinger, C. K. G.; Krüger, S.; Gaich, T. Total Synthesis of Parvineostemonine by Structure Pattern Recognition: A Unified Approach to *Stemona* and *Sarpagine* Alkaloids. *Chem. Eur. J.* **2018**, *24*, 3994-3997.

6. Katritzky, A. R.; Takeuchi, Y. 1,3-Dipolar Character of Six-membered Aromatic Rings. Part I. 1-Methyl-3-oxidopyridinium. *J. Chem. Soc. (C)* **1971**, 874-877.

7. Dennis, N.; Ibrahim, B.; Katritzky, A. R. 1,3-Dipolar Character of Six-membered Aromatic Rings. Part XXI. Thermal Cycloadditions of 1-(5-Nitro-2-pyridyl)- and 1-(4,6-Dimethyl-pyrimidin-2-yl)-3-oxidopyridinium with 2, 4, and 6 π-Electron Components. *J. Chem. Soc. Perkin 1*, **1976**, 2307-2328.

8. Kuthanapillil, J. M.; Thulasi, S.; Rajan, R.; Krishnan, K. S.; Suresh, E.; Radhakrishnan, K. V. Expeditious synthesis of *N*-bridged heterocycles via dipolar cycloaddition of pentafulvenes with 3-oxidopyridinium betaines. *Tetrahedron* **2011**, *67*, 1272-1280.

9. This method was demonstrated to be effective for the computational analysis of the (5+2) cycloaddition of closely related oxidopyrylium species: Yamamoto, Y.; Nakazato, Y.; Tadano, R.; Yasui, T. Combined Computational and Experimental Study on [5 + 2] Cycloaddition of 2-Trifluoromethylated Oxidopyrylium Species Leading to 1-(Trifluoromethyl)-8-oxabicyclo[3.2.1]oct-3-en-2-ones. *J. Org. Chem.* **2022**, *87*, 10216-10228.

10. Liu, F.; Paton, R. S.; Kim, S.; Liang, Y.; Houk, K. N. Diels–Alder Reactivities of Strained and Unstrained Cycloalkenes with Normal and Inverse-Electron-Demand Dienes: Activation Barriers and Distortion/Interaction Analysis. *J. Am. Chem. Soc.* **2013**, *135*, 15642-15649.

11. Johnson, E. R.; Keinan, S.; Mori-Sánchez, P.; Contreras-García, J.; Cohen, A. J.; Yang, W. Revealing Noncovalent Interactions. *J. Am. Chem. Soc.* **2010**, *132*, 6498-6506.

12. Dennis, N.; Ibrahim, B.; Katritzky, A. R. 1,3-Dipolar Character of Six-membered Aromatic Rings. Part XX. Preparation and Dimerisation of 1-(5-Nitro-2-pyridyl)- and 1-(4,6-Dimethyl-pyrimidin-2-yl)-3-oxidopyridinium. *J. Chem. Soc. Perkin 1*, **1976**, 2296-2307.

13. (a) Ducrot, P.-H.; Lallemand, J. Y. Structure of the *Calystegines*: new alkaloids of the nortropane family. *Tetrahedron Lett.* **1990**, *31*, 3879-3882. (b) Lomenzo, S. A.; Enmon, J. L.; Troyer, M. C.; Trudell, M. L. A FACILE AND EFFICIENT SYNTHESIS OF (±)-TROPAN-2-ONE. *Synth. Commun.* **1995**, *25*, 3681-3690.

14. Kuthanapillil, J. M.; Nijamudheen, A.; Joseph, N.; Prakash, P.; Suresh, E.; Datta, A. Radhakrishnan, Cycloaddition profile of pentafulvenes with 3-oxidopyrylium betaine: experimental and theoretical investigations. *Tetrahedron* **2013**, *69*, 9751-9760.

15. (a) Burns, J. M.; Boittier, E. D. Pathway Bifurcation in the (4+3)/(5+2)-Cycloaddition of Butadiene and Oxidopyrylium Ylides: The Significance of Molecular Orbital Isosymmetry. *J. Org. Chem.* **2019**, *84*, 5997-6005. (b) Yu, P.; Chen, T. Q.; Yang, Z.; He, C. Q.; Patel, A.; Lam, Y.; Liu, C.-Y.; Houk, K. N. Mecahnisms and Origins of Periselectivity of the Ambimodal [6+4] Cycloadditions of Tropone to Dimethylfulvene. *J. Am. Chem. Soc.* **2017**, *139*, 8251-8258.

16. Fu, C.; Lora, N.; Kirchhoefer, P. L.; Lee, D. R.; Altenhofer, E.; Barnes, C. L.; Hungerford, N. L.; Krenske, E. H.; Harmata, M. (4+3) Cycloaddition Reactions of *N*-

Alkyl Oxidopyridinium Ions. *Angew. Chem. Int. Ed. Engl.* **2017**, *56*, 14682-14687.

17. Gaussian 16, Revision B.01, M. J. Frisch, G. W. Trucks, H. B. Schlegel, G. E. Scuseria, M. A. Robb, J. R. Cheeseman, G. Scalmani, V. Barone, G. A. Petersson, H. Nakatsuji, X. Li, M. Caricato, A. V. Marenich, J. Bloino, B. G. Janesko, R. Gomperts, B. Mennucci, H. P. Hratchian, J. V. Ortiz, A. F. Izmaylov, J. L. Sonnenberg, D. Williams-Young, F. Ding, F. Lipparini, F. Egidi, J. Goings, B. Peng, A. Petrone, T. Henderson, D. Ranasinghe, V. G. Zakrzewski, J. Gao, N. Rega, G. Zheng, W. Liang, M. Hada, M. Ehara, K. Toyota, R. Fukuda, J. Hasegawa, M. Ishida, T. Nakajima, Y. Honda, O. Kitao, H. Nakai, T. Vreven, K. Throssell, J. A. Montgomery, Jr., J. E. Peralta, F. Ogliaro, M. J. Bearpark, J. J. Heyd, E. N. Brothers, K. N. Kudin, V. N. Staroverov, T. A. Keith, R. Kobayashi, J. Normand, K. Raghavachari, A. P. Rendell, J. C. Burant, S. S. Iyengar, J. Tomasi, M. Cossi, J. M. Millam, M. Klene, C. Adamo, R. Cammi, J. W. Ochterski, R. L. Martin, K. Morokuma, O. Farkas, J. B. Foresman, and D. J. Fox, Gaussian, Inc., Wallingford CT, 2016.

18. Chai, J.-D.; Head-Gordon, M. Long-range corrected hybrid density functionals with damped atom–atom dispersion corrections. *Phys. Chem. Chem. Phys.* **2008**, *10*, 6615-

6620.

19. (a) Hehre, W. J.; Ditchfield, R.; Pople, J. A. Self-Consistent Molecular Orbital Methods. XII. Further Extensions of Gaussian-Type Basis Sets for Use in Molecular Orbital Studies of Organic Molecules. *J. Chem. Phys.* **1972**, *56*, 2257-2261. (b) Hariharan, P. C.; Pople, J. A. The influence of polarization functions on molecular orbital hydrogenation energies. *Theor. Chim. Acta* **1973**, *28*, 213-222. (c) Fracl, M. M.; Pietro, W. J.; Hehre, W. J.; Binkley, J. S.; Gordon, M. S.; DeFrees, D. J.; Pople, J. A. Self-consistent molecular orbital methods. XXIII. A polarization-type basis set for second-row elements. *J. Chem. Phys.* **1982**, *77*, 3654-3665.

20. (a) Fukui, K. The Path of Chemical Reactions – The IRC Approach. *Acc. Chem. Res.* **1981**, *14*, 363-368. (b) Gonzalez, C.; Schlegel, H. B. Reaction path following in mass-weighted internal coordinates. *J. Phys. Chem.* **1990**, *94*, 5523-5527.

21. (a) Zhao, Y.; Truhlar, D. G. Density Functionals with Broad Applicability in Chemistry. *Acc. Chem. Res.* **2008**, *41*, 157. (b) Zhao, Y.; Truhlar, D. G. The M06 suite of density functionals for main group thermochemistry, thermochemical kinetics, noncovalent interactions, excited states, and transition elements: two new functionals

and systematic testing of four M06-class functionals and 12 other functionals. *Theor. Chem. Acc.* **2008**, *120*, 215-241.

22. (a) Krishnan, R.; Binkley, J. S.; Seeger, R.; Pople, J. A. Self-consistent molecular prbital methods. XX. A basis set for correlated wave functions. *J. Chem. Phys.* **1980**, *72*, 650-654. (b) McLean, A. D.; Chandler, G. S. Contracted Gaussian basis sets for molecular calculations. I. Second row atoms, $Z = 11–18$. *J. Chem. Phys.* **1980**, *72*, 5639-5648. (c) Frisch, M. J.; Pople, J. A.; Binkley, J. S. Self-consistent molecular orbital methods 25. Supplementary functions for Gaussian basis sets. *J. Chem. Phys.* **1984**, *80*, 3265-3269. (d) Clark, T.; Chandrasekhar, J.; Spitznagel, G. W.; Schleyer, P. v. R. Efficient diffuse function-augmented basis sets for anion calculations. III. The 3-21+G basis set for first-row elements, Li–F. *J. Comp. Chem.* **1983**, *4*, 294-301.

23. Pieniazek, S. N.; Clemente, F. R.; Houk, K. N. Sources of Error in DFT Computations of C−C Bond Formation Thermochemistries: $\pi \rightarrow \sigma$ Transformations and Error Cancellation by DFT Methods. *Angew. Chem. Int. Ed.* **2008**, *47*, 7746-7749.

24. Marenich, A. V.; Cramer, C. J.; Truhlar, D. G. Universal Solvation Model Based on

Solute Electron Density and on a Continuum Model of the Solvent Defined by the Bulk Dielectric Constant and Atomic Surface Tensions. *J. Phys. Chem. B* **2009**, *113*, 6378-6396.

25. CYLview, 1.0b; Legault, C. Y., Université de Sherbrooke, 2009 (http://www.cylview.org).

26. Lu, T.; Chen, F. Multiwfn: A Multifunctional Wavefunction Analyzer. *J. Comput. Chem.* **2012**, *33*, 580-592.

27. VMD for WIN64, Ver. 1.9.4a53; NIH Center for Macromolecular Modeling & Bioinformatics, University of Illinois at Urbana-Champaign; 2021 (https://www.ks.uiuc.edu/Research/vmd/).